











## Many Roads Lead to Lithium: Formation Pathways For Lithium-Rich Red Giants

MARYUM SAYEED <sup>1</sup>, MELISSA K. NESS <sup>1,2</sup>, BENJAMIN T. MONTET <sup>3,4</sup>, MATTEO CANTIELLO <sup>2</sup>,  
ANDREW R. CASEY <sup>3,4,5</sup>, SVEN BUDER <sup>6,7</sup>, MEGAN BEDELL <sup>2</sup>, KATELYN BREIVIK <sup>2</sup>, BRIAN D. METZGER <sup>1,2</sup>,  
SARAH L. MARTELL <sup>3,7</sup> AND LEAH MCGEE-GOLD<sup>8</sup>

<sup>1</sup>*Department of Astronomy, Columbia University, 550 West 120th Street, New York, NY, USA*

<sup>2</sup>*Center for Computational Astrophysics, Flatiron Institute, New York, NY 10010, USA*

<sup>3</sup>*School of Physics, University of New South Wales, Kensington, New South Wales, Australia*

<sup>4</sup>*UNSW Data Science Hub, University of New South Wales, Sydney, NSW 2052, Australia*

<sup>5</sup>*School of Physics & Astronomy, Monash University, Clayton 3800, Victoria, Australia*

<sup>6</sup>*Research School of Astronomy and Astrophysics, Australian National University, Canberra, ACT 0200, Australia*

<sup>7</sup>*Centre of Excellence for Astrophysics in Three Dimensions (ASTRO-3D), Australia*

<sup>8</sup>*Department of Physics and Astronomy, Barnard College, Columbia University, NY 10027, USA*

Submitted to ApJ

### ABSTRACT

Stellar models predict that lithium (Li) inside a star is destroyed during the first dredge-up phase, yet 1.2% of red giant stars are Li-rich. We aim to uncover possible origins of this population, by analysing 1155 Li-rich giants ( $A(\text{Li}) \geq 1.5$ ) in GALAH DR3. To expose peculiar traits of Li-rich stars, we construct a reference sample of Li-normal (doppelgänger) stars with matched evolutionary state and fiducial supernova abundances. Comparing Li-rich and doppelgänger spectra reveals systematic differences in the H- $\alpha$  and Ca-triplet line profiles associated with the velocity broadening measurement. We also find twice as many Li-rich stars appear to be fast rotators (2% with  $v_{\text{broad}} \gtrsim 20 \text{ km s}^{-1}$ ) compared to doppelgängers. On average, Li-rich stars have higher abundances than their doppelgängers, for a subset of elements, and Li-rich stars at the base of RGB have higher mean  $s$ -process abundances ( $\geq 0.05$  dex for Ba, Y, Zr), relative to their doppelgängers. External mass-transfer from *intermediate*-mass AGB companions could explain this signature. Additional companion analysis excludes binaries with mass ratios  $\gtrsim 0.5$  at  $\gtrsim 7$  AU. We also discover that highly Ba-enriched stars are missing from the Li-rich population, possibly due to *low*-mass AGB companions which preclude Li-enrichment. Finally, we confirm a prevalence of Li-rich stars on the red clump that increases with lithium, which supports an evolutionary state mechanism for Li-enhancement. Multiple culprits, including binary spin-up and mass-transfer, are therefore likely mechanisms of Li-enrichment.

*Keywords:* Stars: abundances — stars: red giant — stars: AGB — stars: binary — stars: evolution

### 1. INTRODUCTION

Lithium (Li) enriched red giants remain a long-standing mystery in astrophysics (Wallerstein & Conti 1969; Trimble 1975, 1991). Stellar evolution predicts that atmospheric lithium abundance – determined by the interstellar medium from which the star forms –

remains fixed throughout most of the star’s lifetime, but is destroyed as the star evolves from the main sequence to the red giant phase. During the first dredge-up (FDU) process (Iben 1968), the outer convective layer expands and overlaps with the hotter, Li-depleted inner layers, diluting the surface lithium abundance through mixing. However,  $\sim 1.2\%$  red giants are found to be Li-enhanced (Gao et al. 2019; Casey et al. 2019).

Lithium-enriched red giants were first discovered by Wallerstein & Sneden (1982). Since then, many additional members of this population have been

Corresponding author: Maryum Sayeed  
maryum.sayeed@columbia.edu

detected in the Milky Way field (e.g., Brown et al. 1989; Charbonnel & Balachandran 2000; Balachandran et al. 2000; Reddy & Lambert 2005; Gonzalez et al. 2009; Carlberg et al. 2010; Charbonnel & Lagarde 2010; Kumar et al. 2011; Monaco et al. 2011; Ruchti et al. 2011a; Kirby et al. 2012a; Lebzelter et al. 2012; Martell & Shetrone 2013; Adamów et al. 2014; da Silva et al. 2015; D’Orazi et al. 2015a,b; Casey et al. 2016; Delgado Mena et al. 2016; Kirby et al. 2016; Li et al. 2018; Yan et al. 2018; Casey et al. 2019; Deepak & Reddy 2019; Gao et al. 2019; Singh et al. 2019; Zhou et al. 2019), clusters (e.g., Sanna et al. 2020; Aguilera-Gómez et al. 2016a; Kirby et al. 2016; Aguilera-Gómez et al. 2022; Schiappacasse-Ulloa et al. 2022), and dwarf spheroidal galaxies (e.g., Kirby et al. 2012b). Large-scale spectroscopic surveys have facilitated detailed studies to identify the culprit for Li-rich red giants, such as *Gaia*-ESO (e.g., Casey et al. 2016; Magrini et al. 2021), LAMOST (e.g., Gao et al. 2019; Wheeler et al. 2021; Singh et al. 2019; Yan et al. 2021; Ming-hao et al. 2021; Yan et al. 2022; Zhou et al. 2022), GALAH (e.g., Deepak & Reddy 2019; Gao et al. 2020; Kumar et al. 2020; Deepak et al. 2020; Martell et al. 2021; Soares-Furtado et al. 2021; Chanamé et al. 2022), and RAVE (e.g., Ruchti et al. 2011b).

Several theories have been proposed to explain Li-enrichment, including enhancement due to asymptotic giant branch (AGB) stars (e.g., Cameron & Fowler 1971; Sackmann & Boothroyd 1992), novae (e.g., Vigroux & Arnould 1979; Tajitsu et al. 2015; Izzo et al. 2015; Starrfield et al. 1978; Molaro et al. 2016; Dearborn et al. 1989; Rukeya et al. 2017), and cosmic ray spallation (e.g., Reeves et al. 1970; Olive & Schramm 1992). Others have associated lithium enhancement to a specific stage in stellar evolution (e.g., Kumar et al. 2020; Mallick et al. 2023), or other processes such as rotationally induced mixing (Denissenkov & Herwig 2004), magnetic buoyancy (e.g., Busso et al. 2007; Nordhaus et al. 2008; Guandalini et al. 2009), planetary engulfment (e.g., Alexander 1967; Siess & Livio 1999a,b; Villaver & Livio 2009; Adamów et al. 2012), and substellar companions (e.g., King et al. 1997; Israelian et al. 2004, 2009; Delgado Mena et al. 2014).

Recent studies have associated specific formation mechanisms to certain stages of stellar evolution. Casey et al. (2019) suggested that planetary engulfment can only account for  $\sim 20\%$  of Li-rich red giants, specifically those early on in the red giant phase. Similarly, Soares-Furtado et al. (2021) used stellar evolutionary models to show that planetary engulfment is only detectable for certain evolutionary states, while Kumar et al. (2020) suggested a universal lithium production event in low-

mass stars between the tip of red giant branch and the red clump.

A popular theory as to the origin of enrichment is lithium production via the Cameron-Fowler mechanism (Cameron & Fowler 1971) where helium isotopes,  $^3\text{He}$  and  $^4\text{He}$ , must fuse together at high temperatures to produce beryllium-7 ( $^7\text{Be}$ ). However, in order to produce Li-7 ( $^7\text{Li}$ ),  $^7\text{Be}$  must be transported to cooler regions to create lithium via electron capture. If the surroundings are not cool enough, the lithium is destroyed by proton capture to produce unstable  $^8\text{Be}$ , which further breaks down into two  $^4\text{He}$  atoms.

Motivated by the large overlap of all-sky spectroscopic and photometric surveys, we take advantage of the newly available GALAH DR3 data to examine signatures of Li-rich stars that might inform their formation mechanisms (Buder et al. 2021). The GALAH survey is especially useful as it provides measured element abundances in five nucleosynthetic families for  $\sim 10^6$  stars near the Sun (De Silva et al. 2015). The provided spectral regions include the lithium and H- $\alpha$  lines, where the latter is a diagnostic of activity and rotation.

In our analysis, we use a reference sample of Li-normal stars to search for empirical differences in Li-rich giants compared to Li-normal stars. We examine features directly in the spectrum itself, in particular the absorption features that are associated with chromospheric activity. We compare the prevalence of Li-enrichment as a function of evolutionary state, and examine the differences in the distributions of stellar parameters not used to construct the reference and Li-rich samples. We perform a detailed analysis of the individual abundances of Li-rich stars compared to Li-normal stars, with a focus on the *s*-process elements, to connect to the role of mass-transfer from AGB stars. We also use the individual abundances to undertake an investigation of condensation temperature trends in the Li-rich sample relative to Li-normal stars, since condensation temperature trends have been associated with planet formation (e.g., Meléndez et al. 2009; Ramírez et al. 2009; Gonzalez et al. 2010).

Our analysis uses not only GALAH but an ensemble of complementary information. This includes spectra in other wavelength regions as well as stellar parameters from *Gaia* and GALEX, for stars common with GALAH. This ensemble of information has only become recently available. Its inclusion maximises the breadth of our pursuit for clues as to the formation mechanisms for Li-enrichment in giants. By combining newly available data and complementary surveys, we see evidence for multiple mechanisms for Li-enrichment.

The paper is organized as follows. We outline the data and methods of sample construction in Section 2. We present the main findings in Section 3: evolutionary state dependence in 3.1, spectral analysis in 3.2, evidence of stellar rotation in 3.3, differences in chemical abundances in 3.4, and condensation temperature trends in 3.5. In Section 4, we discuss the four primary results of our analysis.

## 2. OBSERVATIONS & METHODS

### 2.1. Ground-Based Spectroscopy

Galactic Archaeology with HERMES (GALAH; De Silva et al. 2015) is a high-resolution spectroscopic survey of the southern sky on the Anglo-Australian Telescope. GALAH employs the High Efficiency and Resolution Multi-Element Spectrograph (HERMES; Sheinis et al. 2015) that provides high-resolution ( $R \approx 28,000$ ) spectra in four wavelength bands (4713 – 4903, 5648 – 5873, 6478 – 6737, and 7585 – 7887 Å). For our analysis, we use the latest data release (Buder et al. 2021, GALAH DR3) that provides one-dimensional spectra, stellar atmospheric parameters, and up to 30 individual element abundances for 678,423 spectra of 588,571 mostly nearby stars.

Critically, GALAH spectra covers the strong lithium absorption feature at  $\sim 6708$  Å, and GALAH serves as our primary data set for investigation of Li-rich stars, where a lithium abundance,  $[\text{Li}/\text{Fe}]$ , was measured for 402,901 stars. Using a reference Li-normal sample that we construct, we look for differences that exist in Li-rich stellar spectra, and derived properties, including abundances and rotation. We do this in concert with other spectroscopic and photometric survey data. We also complement the main GALAH catalog with stellar ages, masses, and distances derived using Bayesian Stellar Parameter Estimation code (BSTEP) in Sharma et al. (2018).

### 2.2. Sample Construction

Standard nomenclature for Li-abundance,  $A(\text{Li})$  is defined as the logarithmic abundance of lithium:  $A(\text{Li}) = \log_{10}(N_{\text{Li}}/N_{\text{H}}) + 12$ , where  $N_{\text{Li}}$  and  $N_{\text{H}}$  refer to the number densities of atoms of lithium and hydrogen, respectively. From measurements of  $[\text{Li}/\text{Fe}]$  and  $[\text{Fe}/\text{H}]$ , we calculate the absolute lithium abundance as  $A(\text{Li}) = [\text{Li}/\text{Fe}] + [\text{Fe}/\text{H}] + 1.05$ , where 1.05 is the solar photospheric lithium abundance (Asplund et al. 2009). Thresholds to define Li-enrichment vary (e.g., Aguilera-Gómez et al. 2016b,a; Deepak & Reddy 2019; Kumar et al. 2020); here, we adopt the traditional limit of  $A(\text{Li}) \geq 1.5$  which is the mean post dredge-up value predicted by standard evolution for Population I stars.

To select Li-rich stars in GALAH across the sky, we follow the criteria outlined in Martell et al. (2021). We briefly summarize the steps below and direct the reader to Section 2.2 of Martell et al. (2021) for more details. Similar to their conditions, stars in our sample have:

- i) a surface gravity  $\log g \in [-1.0, 3.2]$  dex
- ii) an effective temperature  $T_{\text{eff}} \in [3000, 5730]$  K
- iii) quality flags with no known problems in the spectrum, nor  $[\text{Fe}/\text{H}]$  and  $[\text{Li}/\text{Fe}]$  measurements: `flag_sp <= 1, flag_fe_h = 0 & flag_Li_fe = 0`
- iv) *WISE*  $W_2$  band data quality flag of A, B, or C
- v) been excluded from LMC and SMC
- vi)  $E(B - V) < 0.33$

Out of a total of 588,571 stars in GALAH DR3<sup>1</sup>, 11,256 stars satisfy the above conditions. We then divide the resulting sample into Li-rich and Li-normal groups, where ‘Li-rich’ stars have a  $A(\text{Li})$  above 1.5 dex, and ‘Li-normal’ (or ‘doppelgänger’) stars have  $A(\text{Li})$  below 1.0 dex. This results in 1455 Li-rich and 7543 Li-normal stars.

We then find a doppelgänger from the available 7543 stars for each 1455 Li-rich star. We select the doppelgänger for each Li-rich star with the minimum distance in four-dimensional parameter space, where the four stellar parameters are  $T_{\text{eff}}$ ,  $\log g$ ,  $[\text{Fe}/\text{H}]$  and  $[\text{Mg}/\text{Fe}]$ . Given the large set of field stars we have, this nominally selects for each Li-rich star a reference object with the same evolutionary state and overall metallicity from core collapse and thermonuclear supernovae. To do this, we use the  $\chi^2$  distance metric shown in Equation 1 for each Li-rich star,

$$\min \sum_{i=1}^4 \frac{(x_{R,i} - x_{N,i})^2}{\sigma_{R,i}^2 + \sigma_{N,i}^2} \quad (1)$$

where  $x_{R,i}$  is the value of the  $i$ th stellar parameter for the Li-rich star (ie.  $T_{\text{eff}}$ ),  $x_{N,i}$  is the same stellar parameter but for the Li-normal star, and  $\sigma_{R,i}$  and  $\sigma_{N,i}$  are the uncertainties on the parameters for the Li-rich and Li-normal stars, respectively.

However, to ensure our pairs are similar in these four parameter dimensions, we also require from the doppelgängers that the difference in each parameter between Li-rich and Li-normal star is less than the mean error in each parameter. The mean errors are constructed using the sample of 1455 Li-rich stars, which in  $T_{\text{eff}}$ ,  $\log g$ ,  $[\text{Fe}/\text{H}]$ , and  $[\text{Mg}/\text{Fe}]$  are 100 K, 0.45 dex, 0.08 dex and 0.09 dex, respectively. This additional step ensures the doppelgängers are the same as their

<sup>1</sup> [https://www.galah-survey.org/dr3/the\\_catalogues/](https://www.galah-survey.org/dr3/the_catalogues/)

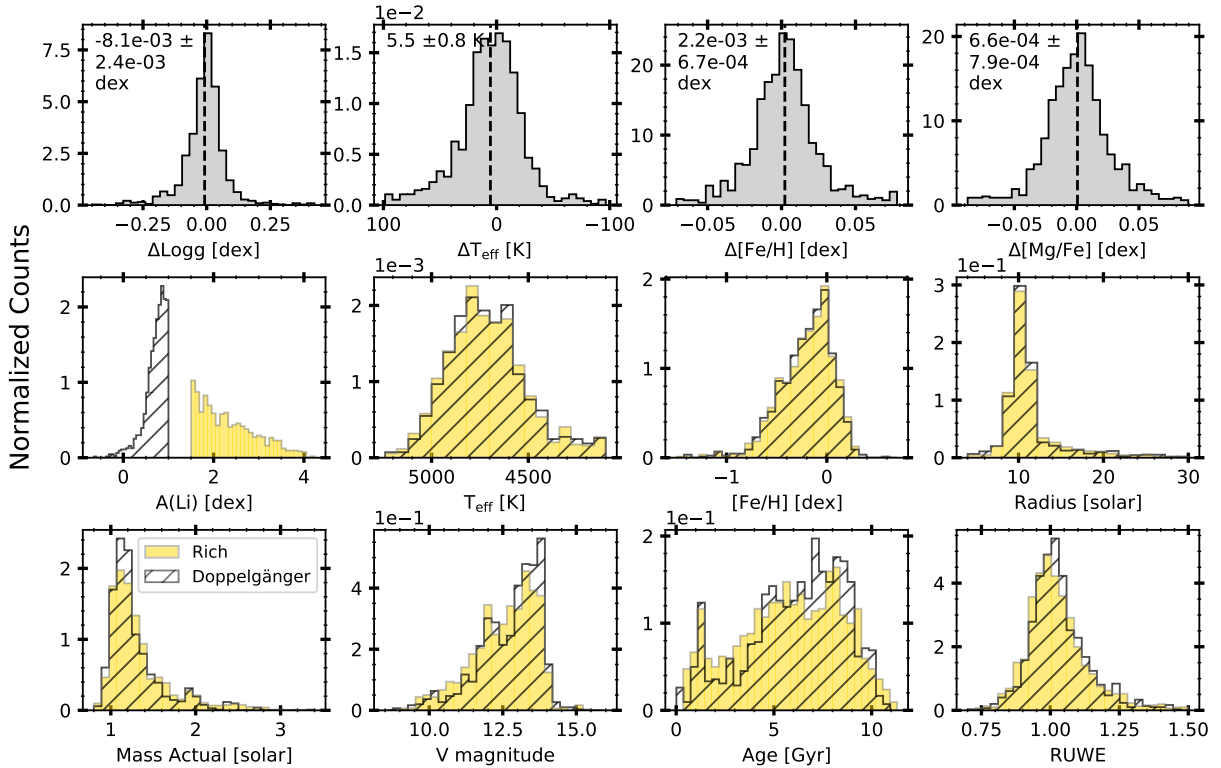


**Figure 1.** *Top row:* Normalized histograms showing the difference in stellar properties from GALAH –  $T_{\text{eff}}$ ,  $\log g$ ,  $[\text{Fe}/\text{H}]$ , and  $[\text{Mg}/\text{Fe}]$  – between Li-rich stars and their doppelgängers. The doppelgängers are selected using these parameters, and have near mean zero differences and standard deviations below the uncertainties on the parameters. The text indicates the mean difference, also designated by the dashed line, and its associated error. *Middle & bottom row:* The first column in the middle row shows the distribution of lithium in the two samples. The remaining sub-panels show the normalized histograms of different parameters for the Li-rich (yellow) and doppelgänger (grey) samples in GALAH. Apart from the lithium abundance, the samples are very well matched. Note that a small fraction of the 1155 stars falls outside of the figure shown, namely 23 stars in the radius distribution, 1 star in the  $V$  magnitude distribution, and 29 stars in the RUWE distribution.

Li-rich stars in the four parameters, within the typical uncertainties. Of the 1455 Li-rich stars, 1155 stars satisfied this criteria. Table 1 contains the GALAH IDs for both Li-rich stars and the 830 doppelgängers in the final sample of 1155 Li-rich stars. Note that some Li-rich star share the same doppelgänger.

Figure 1 summarizes the stellar properties of the Li-rich and Li-normal samples, showing that the Li-normal sample is an accurate reflection of the Li-rich sample for all stellar parameters. The top row of Figure 1 shows the distribution of the differences in the chosen parameters:  $T_{\text{eff}}$ ,  $\log g$ ,  $[\text{Fe}/\text{H}]$ , and  $[\text{Mg}/\text{Fe}]$ . The mean difference in inferred  $T_{\text{eff}}$  is  $\sim 5$  K, and less than 0.01 dex in  $\log g$ ,  $[\text{Fe}/\text{H}]$ , and  $[\text{Mg}/\text{Fe}]$ .

Our sample includes stars in different evolutionary states. We subsequently examine our sample at the following evolutionary points: the base of the red giant branch, the red clump and the red giant branch. Prior work has suggested mechanisms of enrichment that are uniquely at the red clump stage (e.g., Deepak & Reddy

2019; Martell et al. 2021; Deepak & Lambert 2021a,b). Singh et al. (2019). To classify the stars in our sample as red clump or red giant members, we follow the criteria outlined in Martell et al. (2021), and use existing GALAH flags that have already categorised stars into an evolutionary state. This has been done following a Bayesian classification pipeline (Sharma et al. 2018) where,

- red clump (RC) stars have  $\text{is\_redclump\_bstep} \geq 0.5$  and  $|W_2 + 1.63| \leq 0.80$
- red giant branch (RGB) stars have  $\text{is\_redclump\_bstep} < 0.50$  and  $|W_2 + 1.63| > 0.80$
- base of RGB stars have  $\log g \geq 2.7$  dex

Note that stars at the base of RGB are a subset of RGB stars, such that they pass the RGB selection, but they also have  $\log g \geq 2.7$  dex. Implementing these conditions results in 134 RGB stars, 698 RC stars, and 90 base of RGB stars, where the mean  $A(\text{Li})$  is  $2.1 \pm 0.5$  dex,  $2.4 \pm 0.7$  dex, and  $2.1 \pm 0.5$  dex, respectively.

**Table 1.** GALAH ID for Li-rich stars and their doppelgängers.

Rich	Doppelgänger
131118002901313	160420006901346
131123003501064	150831002501056
131218002401174	170122002601232
140112002301046	161013005401342
140209002201006	150209002201337
140209002202072	160123002601071
140303000402167	161006002601323
140307003101263	140811002701001
140309003101259	140805002601204
140309003101316	170215004601063
...	...

**Table 2.** *Gaia* DR3 ID for 667 Li-rich stars and their doppelgängers with *Gaia* RVS spectra.

Rich	Doppelgänger
1753307668590290304	6418518737689993216
2535920013509617152	5361465232463833856
2536027971807637248	598955115237068032
2549549422208614912	5806683707030940416
2549897589437503488	4962188545583682560
2597169751843870336	6155086776853130496
2608309007224057856	6743712358307891328
2613265021526634624	4624378303918945920
2622394708952964096	3601040910434367744
2679552786563683328	6145487391806151936
...	...

### 2.3. *Gaia* DR3 & GALEX

We also use *Gaia* data for our sample of GALAH stars to analyze regions of the stellar spectra not covered by GALAH. *Gaia* Data Release 3 (DR3) provides near-infrared (845–872 nm) spectra at medium-resolution ( $R \approx 11,500$ ), measured with the Radial Velocity Spectrometer (RVS) for 999,645 sources and centered on the Ca-triplet (Gaia Collaboration et al. 2016; Cropper et al. 2018; Gaia Collaboration et al. 2022). The Ca-triplet core is particularly interesting as a marker of magnetic activity in the upper layers of the chromosphere (Lanzafame et al. 2022). We therefore wish to compare this feature in Li-rich and Li-normal stars. We find 673 stars in our Li-rich sample with available RVS spectra.

We find doppelgängers for these stars in *Gaia* spectra in order to compare the Ca-triplet feature in the two samples; however, we now use the spectra to find doppelgängers, rather than the stellar parameters. While we can not explicitly select only Li-normal stars in our reference doppelgänger set, as there is no lithium measurement from *Gaia*, the candidate doppelgängers are most likely to be Li-normal, given that only  $\sim 1\%$  of giants are Li-rich. The criteria and steps taken to create the doppelgänger sample are described below:

- i) We remove the 673 Li-rich from the RVS catalog; 998,972 stars remain.
- ii) To reduce the search space for doppelgängers for each Li-rich object, we generate a list of possible doppelgängers for each Li-rich star with differences in  $T_{\text{eff}}$  and  $[\text{Fe}/\text{H}]$  between the Li-rich

and doppelgänger within the mean uncertainties ( $< 100$  K for  $T_{\text{eff}}$  and  $< 0.15$  dex for  $[\text{Fe}/\text{H}]$ ). We also ensure the signal-to-noise (SNR) of the doppelgänger is above 50; this results in a list of 182,898 possible doppelgängers for all 673 Li-rich stars.

- iii) We use a  $\chi^2$  distance metric on the spectra but exclude the Ca-triplet region. We compare each Li-rich star to the subset of candidate doppelgänger stars using this distance metric, arriving at a  $\chi^2$  distance for each possible doppelgänger for each Li-rich star. The numerator terms are the normalised flux of the pair of stars and the denominator terms are the corresponding flux uncertainties. The wavelength regions we calculate this over are 8477 – 8492 Å, 8507 – 8532 Å, and 8600 – 8653 Å. For each Li-rich star, we find a set of doppelgänger stars with a reduced  $\chi^2$  value below 2 times the degrees of freedom (ie.  $2 \times N_{\lambda}$ ).
- iv) For all doppelgänger stars that satisfy the above condition, we select a random star from the shortlist as the doppelgänger, resulting in a final 667 Li-rich stars with *Gaia* RVS spectra matched with a doppelgänger.

Table 2 contains the *Gaia* DR3 IDs for the 667 Li-rich stars and their doppelgängers with *Gaia* RVS spectra.

Furthermore, to search for any Li-rich objects with significant signatures of stellar activity, we also look for emission in the ultraviolet (UV). We use NASA’s Galaxy Evolution Explorer (GALEX), and its associated All-Sky Imaging Survey (AIS), to examine the UV emission

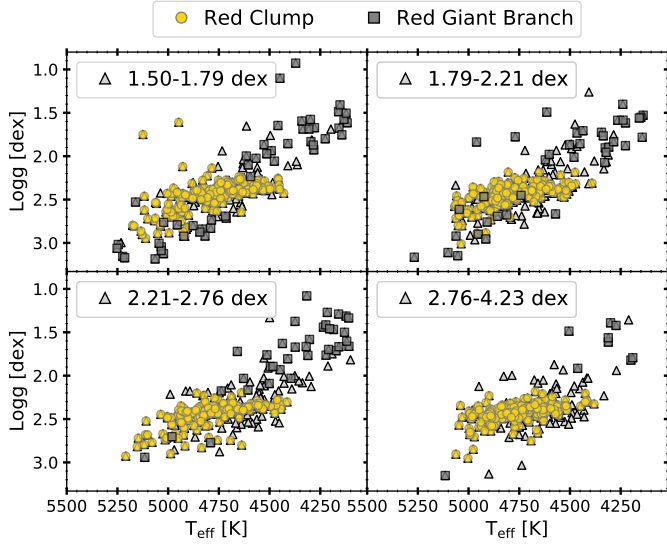


**Figure 2.** Kiel diagram of Li-rich stars divided into four equal bins of lithium abundance where the  $A(\text{Li})$  of data points in each subplot is indicated in the legend. The grey squares and yellow circles show stars on the red giant branch and red clump, respectively, based on criteria from [Martell et al. \(2021\)](#). The distribution of  $\log g$  of stars in our sample becomes more centered around  $\log g$  of  $\sim 2.4$  dex as stars become more Li-rich, indicating that super-Li-rich stars are more likely to be red clump stars. Also see [Figure 3](#).

in our stars ([Martin et al. 2005](#); [Bianchi et al. 2017](#)). Within GALEX<sup>2</sup>, we find 332 of our Li-rich and 330 Li-normal stars. Object IDs from the three surveys mentioned – GALAH, *Gaia* and GALEX – are included in [Tables 5 and 6](#) for the Li-rich and doppelgänger samples.

### 3. RESULTS

We summarize our findings in five main results:

- i) preferential red clump membership as a function of Li-enrichment,
- ii) evidence of net differences in the H- $\alpha$  and Ca-triplet line profiles,
- iii) differences in the mean rotation of a subset of Li-rich giants relative to their doppelgänger,
- iv) difference in mean element abundances for some elements for the Li-rich population, in particular signatures in neutron-capture elements and at the base of the red giant branch, and a ‘missing’ population of Ba-enriched stars, and

<sup>2</sup> using MAST to cross-reference our samples with GR6+7 from all catalogs (AIS, MIS, DIS)

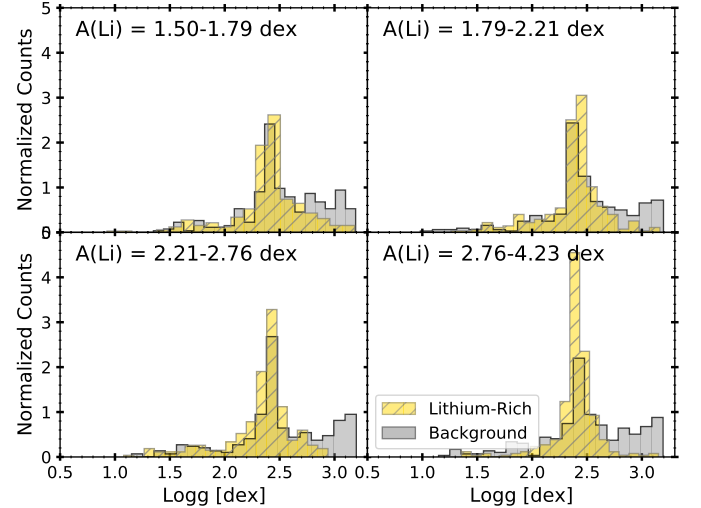


**Figure 3.** Histograms showing randomly sampled  $\log g$  in GALAH in four bins of lithium abundance to demonstrate that the background GALAH sample is not preferentially centered at a specific  $\log g$ , and that our finding that red clump stars are more likely to be Li-rich (shown in [Figure 2](#)) is real.

- v) absence of any difference between the Li-rich and Li-normal stars’ trends in condensation temperature ranked element abundance values.

#### 3.1. Evolutionary State Analysis

To investigate the correlation between evolutionary state and Li-enhancement, we divide our sample of Li-rich stars into bins of lithium with equivalent numbers of stars within each bin, shown on a Kiel diagram in [Figure 2](#). We see that the most Li-rich stars (ie.  $A(\text{Li}) = 2.8 - 4.2$ ) are preferentially red clump stars. In fact, we see overall that as the  $A(\text{Li})$  increases, a larger relative fraction of the stars fall on the clump. More specifically, the fraction of RGB stars decreases from 17% to 3%, while the fraction of RC stars increases from 58% to 67%, for higher lithium abundances.

Moreover, in [Figure 3](#) we show that this trend is not due to the survey selection function. To demonstrate this, we select GALAH stars with a  $T_{\text{eff}}$  and  $\log g$  range of our Li-rich sample, and randomly sample 1155 ‘background’ stars in GALAH from a sample of 111,214 total stars, repeated 100 times. As seen in [Figure 3](#), we see that the background sample is not preferentially centered at a given  $\log g$  as a function of lithium abundance, contrary to our Li-rich sample. Therefore, our finding of increasing numbers of red clump stars at higher lithium abundance in [Figure 2](#) is not a consequence of GALAH’s selection function.

#### 3.2. Spectral Analysis

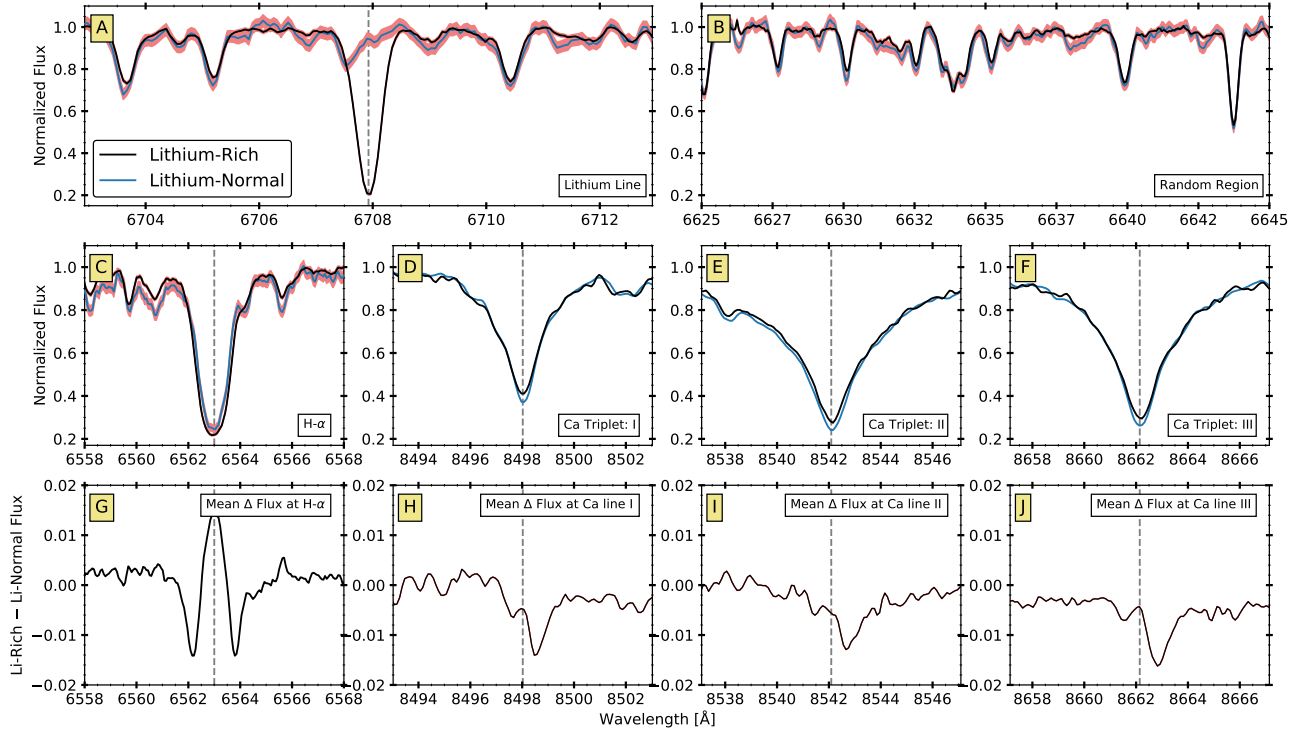


**Figure 4.** Examples of spectra from GALAH and *Gaia* of Li-rich and doppelgänger pairs. Plots A, B, C and G show GALAH spectra, and plots D-F and H-J show *Gaia* RVS spectra. The black and blue curves show data for Li-rich and Li-normal stars, respectively. The red shaded region represents the reported uncertainty on the flux. The chosen Li-rich star is the same in GALAH and *Gaia* (GALAH ID: 160919001601113 or *Gaia* DR3 ID: 6731814646069597312), but its doppelgänger is different between GALAH and *Gaia* (GALAH doppelgänger 150824003101067 and *Gaia* doppelgänger 4645560223628754816). **Panel A:** region of GALAH spectra centered around the Li-line at 6707.926 Å; the Li-rich star clearly has a strong lithium absorption feature not present in the Li-normal star. **Panel B:** arbitrary region of GALAH spectra to show the spectra look nearly identical. **Panel C:** GALAH spectra centered around the H- $\alpha$  line at 6562.79 Å. **Panel D, E, F:** *Gaia* spectra centered on the Ca-triplet lines. **Panel G:** average difference in flux for all 1155 Li-rich and Li-normal stars in GALAH. **Panel H, I, J:** average difference in flux at the Ca-triplet lines between all 667 Li-rich and Li-normal stars in *Gaia* with available *Gaia* RVS data. The error in flux is plotted under each curve.

The GALAH and *Gaia* spectra have features – notably the H- $\alpha$  and Ca H & K lines, respectively – that can probe emission and chromospheric activity, and reveal stellar rotation due to their broad and strong line profiles that are formed in the chromosphere. We examine these features in the Li-rich and Li-normal samples. In Figure 4, we show examples of spectra centered around the lithium and H- $\alpha$  lines in GALAH, and the Ca-triplet in *Gaia*. In Panels G-J, we show the difference in flux between Li-rich and Li-normal stars averaged over the complete sample (ie. 1155 in GALAH and 667 in *Gaia*), thereby reducing the sampling noise at each wavelength to  $\sim 0.0003$  at a typical wavelength for GALAH, and  $\sim 0.002$  for *Gaia*. We see statistically significant differences at the H- $\alpha$  and Ca-triplet lines, and an asymmetry in the latter which could be caused by surface velocity structure (e.g., Gray 1980; Mallik 1997; Nieminen 2017). These profiles in Panels G-J are potentially consistent with systematic differences in

activity in the stellar chromosphere (e.g., Sneden et al. 2022), differences in stellar rotation, or binary fractions between the Li-rich and reference samples; all would manifest in similar profiles seen in the bottom panel of Figure 1.

If the Cameron-Fowler mechanism is responsible for Li-enriched stars, this should also correspondingly enhance another product of the reaction, namely beryllium (Cameron & Fowler 1971). By pooling our spectra, we attempted to detect any small differences in absorption strength at the beryllium line<sup>3</sup> at 4828.159 Å between the Li-rich and Li-normal stars. Despite stacking spectra of 1155 Li-rich stars to increase the signal, we made no detection of beryllium. However, there have been detections of beryllium in stars, but at a

<sup>3</sup> From NIST: <https://physics.nist.gov/PhysRefData/Handbook/Tables/berylliumtable2.htm>

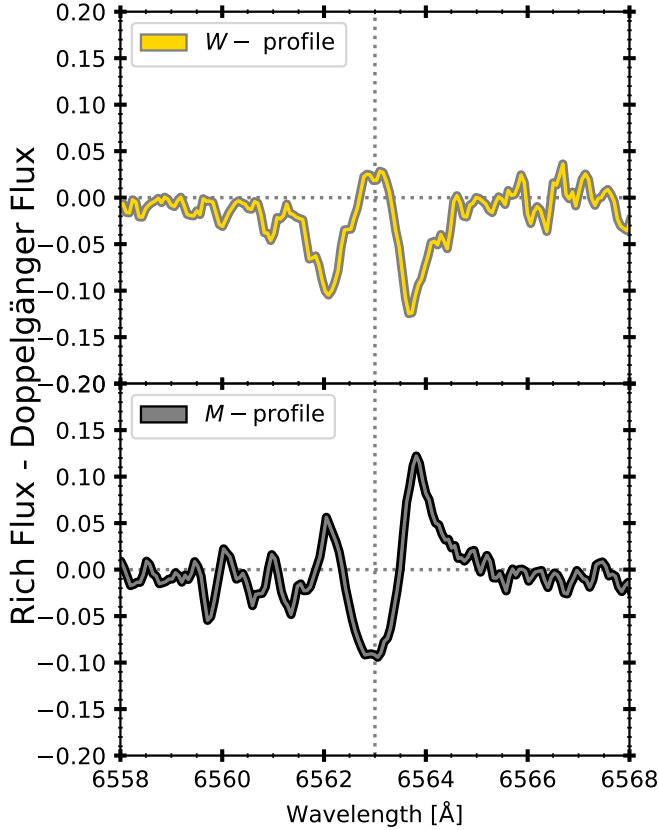


**Figure 5.** Difference in spectral flux between Li-rich and doppelgänger star centered on the H- $\alpha$  line. *Top:* a pair of Li-rich and doppelgänger where the resulting spectrum creates a *W*-profile, corresponding to a Li-rich star with emission in the core relative to its doppelgänger, and with deeper absorption either side. *Bottom:* a pair of Li-rich and doppelgänger where the resulting spectrum creates a *M*-profile, corresponding to a Li-rich star with emission in the wings relative to its doppelgänger, and with deeper absorption in the core.

line not within the GALAH spectral range (e.g., Gilmore et al. 1991; Boesgaard & Krugler Hollek 2009; Giribaldi & Smiljanic 2022; Smiljanic et al. 2022).

### 3.2.1. H- $\alpha$ Line Profiles

Panel G of Figure 4 shows the mean difference in the core of the H- $\alpha$  line in the Li-rich stars as compared to their doppelgängers. To investigate this finding in more detail, we examine this H- $\alpha$  feature as a function of [Fe/H] and  $A(\text{Li})$  for both Li-rich and Li-normal stars, but find no significant dependence of [Fe/H] and  $A(\text{Li})$  on the H- $\alpha$  feature when binning in [Fe/H] and  $A(\text{Li})$ .

However, by examining the difference in the spectra for individual pairs in more detail, we noticed differing shapes of the spectrum at the H- $\alpha$  line. We subsequently categorized each pair difference into a *W*-profile,

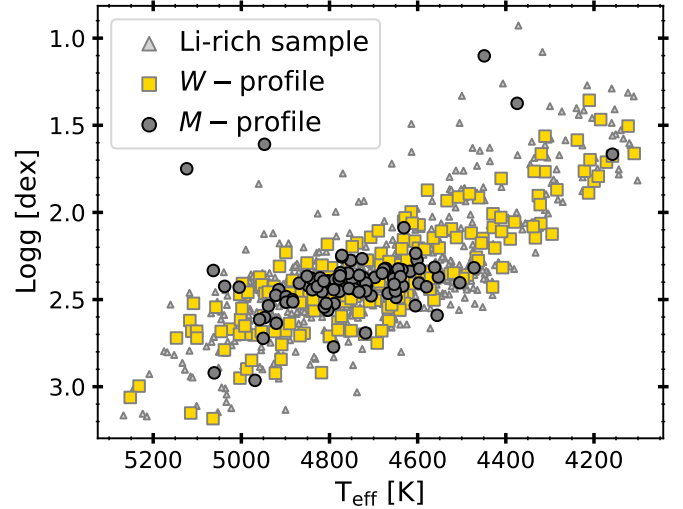


**Figure 6.** Stars classified as *W*- or *M*- in the Li-rich sample on a Kiel diagram.

*M*-profile, or neither. Of our 1155 Li-rich stars, 19% of the sample (218 stars) produced a *W*-profile with their doppelgänger, 8% of the sample (87 stars) produced an *M*-profile, and 73% were unclassified. We show an example of a *W*-profile and *M*-profile in Figure 5, and show the distribution of *W* and *M* designations on a Kiel diagram in Figure 6. Interestingly, almost all the *M*-designations fall on the red clump, at  $\log g \sim 2.4$  dex, while the *W*-designations span the entire giant branch.

As seen in Figure 5, *W*-designations correspond to deeper flux in the wings in the Li-rich stars and higher flux in the core, while *M*-designations refer to deeper flux in the core and higher flux in the wings for the Li-rich star. Based on spectral shapes, these differences could be explained by respectively faster rotation of the Li-rich star compared to the doppelgänger (*W*-profile), and slower rotation of the Li-rich star compared to the doppelgänger (*M*-profile). The *W* and *M* profiles would also be produced if one of the pairs is in a (barely-detectable) spectroscopic binary, the *W*-profile when the Li-rich star is a binary and the *M*-profile when the doppelgänger is a binary; we investigate this further in Section 4.2.1. Interestingly, these profiles show asymmetry around the center of the line, with the higher wavelength wing profile of the *M*-designations showing a larger difference than the lower wavelength wing.

Similarly, we inspect differences in the *Gaia* RVS spectra between the Li-rich and Li-normal stars around the Ca-triplet lines. We similarly classify the differences into *W* or *M* through visual inspection. This categorizes  $\sim 8\%$  (51 stars) as *W* relative to the doppelgänger,  $\sim 6\%$



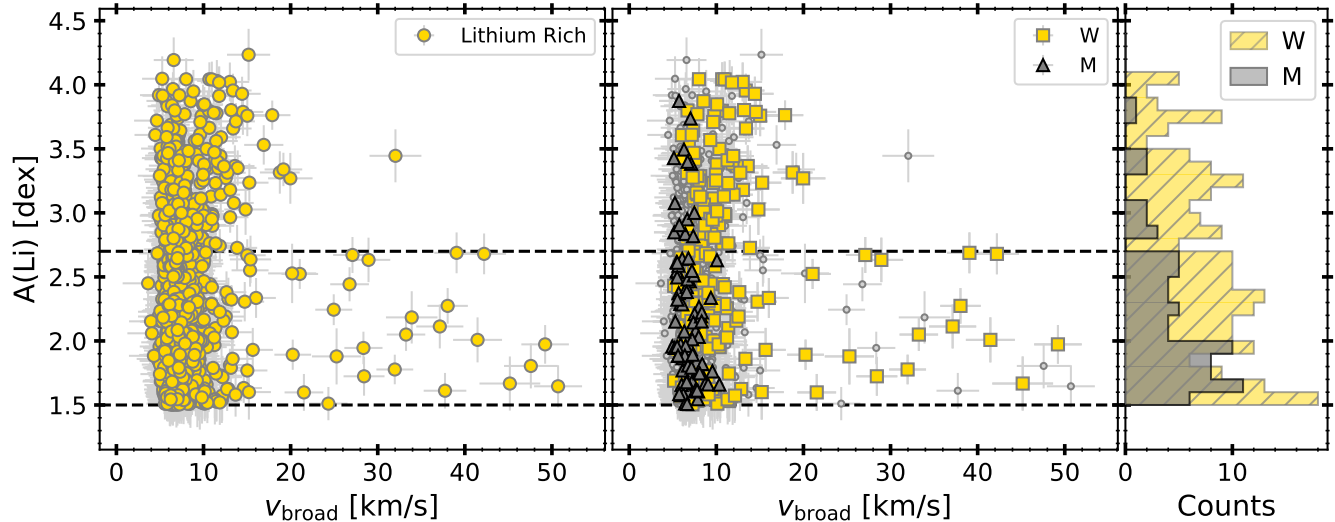


**Figure 7.** Distribution of lithium abundance,  $A(\text{Li})$ , as a function of  $v_{\text{broad}}$  (in  $\text{km s}^{-1}$ ). *Left:* data points show the Li-rich sample. *Middle:* same sample as left panel, separated into stars that create  $W$ -profiles (yellow squares) or  $M$ -profiles (grey triangles) in their  $\text{H}\alpha$  doppelgänger difference. The dashed lines at  $A(\text{Li}) = 1.5$  dex and  $A(\text{Li}) = 2.7$  dex are shown for reference. *Right:* distribution of the two profiles –  $W$  and  $M$  – as a function of  $A(\text{Li})$ . Stars with  $W$ -profiles have higher  $v_{\text{broad}}$  as compared to stars with  $M$ -profiles. This makes physical sense as deeper wing profiles correspond to faster rotation.

(42 stars) as  $M$  relative to the doppelgänger, and the rest as unclassified. Of the 218  $W$ -designations at the  $\text{H}\alpha$  line, 15 also have  $W$ -designation at the Ca-triplet, and of the 87  $M$ -designations at the  $\text{H}\alpha$  line, 3 also have  $M$ -designation at the Ca-triplet.

These differences in the line profiles in both the  $\text{H}\alpha$  and Ca-triplet between the Li-rich stars and their doppelgängers could be rotation driven (e.g., shallower and broader lines), and we directly investigate the measured rotation in the next section. Under this interpretation, the higher fraction of  $W$ -profiles ( $\sim 2:1$ ) is consistent with a fraction of Li-rich stars having a net faster rotation than their Li-normal counterparts in the overall population. Conversely, binarity could masquerade as a measured faster rotation for a single star. However, further follow up work with additional survey data with multi epoch spectra is needed to differentiate between these scenarios.

### 3.3. Stellar Rotation Rate

#### 3.3.1. $v_{\text{broad}}$

Since the spectra indicate the possibility of some rotation differences between the Li-rich and Li-normal samples, we examine the rotation of the Li-rich and Li-normal samples via the broadening velocity ( $v_{\text{broad}}$ ) measurement for each star. GALAH provides  $v_{\text{broad}}$  measurements which encompasses macroturbulence and rotational velocities (fitted with  $v \sin i$ ). This indicates a subtle signature of a fraction of faster rotators in the Li-rich population. Note that we have confirmed that

the rotational broadening estimates, which could serve as a parameter to model the empirical resolution of the data, show no systematic difference with observing date, and between Li-rich and Li-normal samples.

Figure 7 shows the distribution of Li-rich stars as a function of  $v_{\text{broad}}$  for the complete sample,  $W$  and  $M$  profiles, and Figure 8 shows corresponding distribution for the doppelgängers (similar to the left panel of Figure 7). From Figures 7 and 8, the vast majority of stars in both the Li-rich and doppelgänger populations, have a measured  $v_{\text{broad}} \sim 5 - 15 \text{ km s}^{-1}$  (with typical  $v_{\text{broad}}$  measurement uncertainties of  $\sim 2 \text{ km s}^{-1}$ ). However, we see a very small fraction of anomalously high rotators. In fact, we find twice as many fast rotators in the Li-rich sample compared to the doppelgänger population; in the Li-rich sample,  $\sim 2.2\%$  of the stars have  $v_{\text{broad}} \geq 20 \text{ km s}^{-1}$  (26/1155), compared to only 0.8% in the Li-normal sample (7/830). Following typical classifications, a  $v \sin i \gtrsim 10 \text{ km s}^{-1}$  is commonly defined as a fast rotator on the RGB (e.g., Carney et al. 2008; Patton et al. 2023), which is a generous threshold for fast rotation, but also robustly accounts for measurement uncertainty in the reported  $v_{\text{broad}}$ .

From the middle and right panels of Figure 7, we see a clear difference in the  $v_{\text{broad}}$  distributions of the  $W$  and  $M$  designations.  $W$ -designations show a larger relative fraction of stars with lower lithium enhancement, which are preferentially the stars rotating faster than their doppelgängers. Conversely,  $M$ -designations all fall to the lower boundary of the  $v_{\text{broad}}$  distribution; these are

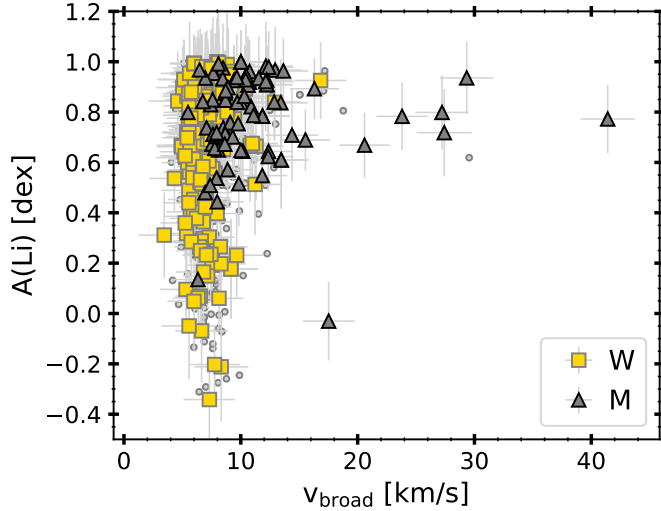


**Figure 8.** Distribution of lithium abundance,  $A(\text{Li})$ , as a function of  $v_{\text{broad}}$  (in  $\text{km s}^{-1}$ ) for doppelgängers, separated into Li-rich stars that show  $W$ -profiles (yellow squares) or  $M$ -profiles (grey triangles) in their  $\text{H}\alpha$  doppelgänger difference. Li-normal stars where their Li-rich counterpart has a  $M$ -profile have high  $v_{\text{broad}}$  than doppelgängers where the Li-rich star has a  $W$ -profile, opposite of the trends seen in the Li-rich population in Figure 7.

the stars for which the Li-rich star is rotating slower than its doppelgänger. The majority of the fast rotators ( $v_{\text{broad}} \geq 20 \text{ km s}^{-1}$ ) are classified using the  $\text{H}\alpha$  feature; of the stars with  $v_{\text{broad}} \geq 20 \text{ km s}^{-1}$ , 68% (15/22) are  $W$ -designations, and 7 are neither, which further suggests that  $W$ -designations are more likely to be Li-rich. In Figure 8, the anomalously high rotators are the reverse designation,  $M$ , as in this case typically the doppelgänger is the faster rotator of the pair.

In Figure 9, we show the fractional difference in  $v_{\text{broad}}$  between the pairs of stars (Li-rich – doppelgänger) for the full sample, and for the two designations,  $W$  and  $M$ . The median fractional difference in  $v_{\text{broad}}$  is  $0.04 \pm 0.01$ ,  $0.30 \pm 0.03$ , and  $-0.37 \pm 0.03$  for the full Li-rich sample,  $W$ -designations and  $M$ -designations, respectively. The net rotation of the Li-rich stars is therefore marginally (4%) higher than the doppelgänger sample, overall.

Figure 9 clearly shows that Li-rich stars with  $W$ -profiles have higher  $v_{\text{broad}}$  relative to their doppelgänger, while Li-rich stars with  $M$ -profiles have a lower  $v_{\text{broad}}$  than their doppelgänger. That is, Li-rich stars that show deeper  $\text{H}\alpha$  wings than their doppelgängers have correspondingly higher rotation, which makes sense as rotation deepens the wings of the  $\text{H}\alpha$  line (Petrenz & Puls 1996). Conversely,  $M$ -designations, which have shallower wings and

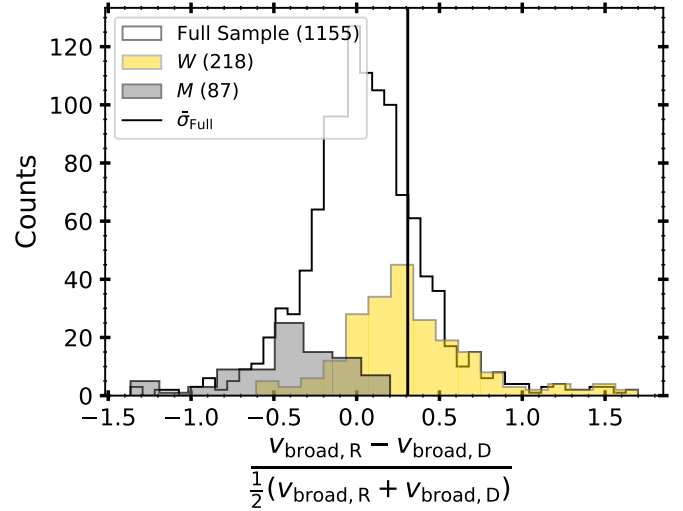


**Figure 9.** Fractional difference in broadening velocity ( $v_{\text{broad}}$ ) between a Li-rich star and its doppelgänger for all stars in our sample (solid black bars), stars with  $W$ -profiles (yellow bars), and stars with  $M$ -profiles (grey bars) in their doppelgänger difference. The solid line shows the  $1-\sigma$  standard deviation expected around a zero mean based on the measurement uncertainty alone for the full sample.

deeper cores in the Li-rich stars compared to their doppelgängers, show lesser broadening. Note that there are more than twice as many  $W$ -designations than  $M$ -designations, which is also expressed as a skew seen in the distribution of the full sample seen Figure 9.

### 3.3.2. UV and IR and Gaia Photometry

Given the well-known correlation between rotation and stellar activity (e.g., Wilson 1966; Kraft 1967; Noyes et al. 1984; Soderblom et al. 1993), we look for any relationship between ultraviolet (UV) emission and lithium abundance. Dixon et al. (2020) derived an empirical relationship between near-UV (NUV) excess and rotational velocity ( $v \sin i$ ) for their sample of 133 stars in APOGEE and GALEX (Ahumada et al. 2020); we use a similar method to look for NUV excess in our Li-rich sample. In Figure 10, we show our Li-rich and doppelgänger sample on a colour-colour diagram. The dotted black line shows the reference UV excess activity (Findeisen & Hillenbrand 2010; Dixon et al. 2020) described by the following:

$$\text{NUV} - J = (10.36 \pm 0.07)(J - K_s) + (2.76 \pm 0.04) \quad (2)$$

We use  $J$  and  $K_s$  measurements from 2MASS, and NUV measurements from GALEX DR6. As seen in Figure 10, we see no difference in the distribution of points between our Li-rich and Li-normal samples.

We also looked for differences in infrared (IR) excess between the Li-rich and Li-normal samples using W1

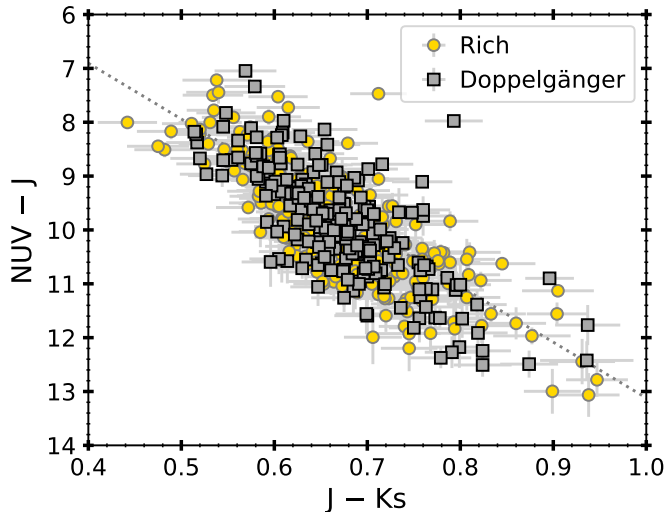


**Figure 10.** Colour-colour diagram of our Li-rich (yellow circles) and Li-normal (grey squares) samples, where the dotted line shows the reference NUV excess. The close overlap in the distribution of the Li-rich and Li-normal samples suggests no UV excess for Li-rich stars detected by GALEX.

and W4 magnitudes from WISE (Cutri & et al. 2012; Rebull et al. 2015), but found no differences in distribution between Li-rich and Li-normal samples, or between *W* and *M* designations. We also checked for indications of photometric variability using *Gaia* DR3 photometry, specifically in the *G*, *G*<sub>BP</sub> (400 – 500 nm) and *G*<sub>RP</sub> (600 – 750 nm) bandpasses. We found no difference in distributions between the Li-rich and doppelgänger samples. Finally, we searched for correlations between lithium abundance and the re-normalized unit weight-error (RUWE). RUWE is the magnitude and colour-independent re-normalization of the astrometric  $\chi^2$  fit in *Gaia* DR2, which is sensitive to close binaries (e.g., Evans et al. 2018; Gaia Collaboration et al. 2018; Lindegren et al. 2018; Berger et al. 2020). In doing a best fit between  $v_{\text{broad}}$  and RUWE, we found no indication that  $v_{\text{broad}}$ , nor  $A(\text{Li})$ , are correlated with RUWE given a negligible slope between  $A(\text{Li})$  vs.  $v_{\text{broad}}$ , and  $A(\text{Li})$  vs. RUWE.

### 3.4. Abundance Analysis

The multiple individual abundances measured for GALAH enables us to compare the distribution of abundances between Li-rich and doppelgänger samples. We examine the following elements: Al,  $\alpha$ , Ba, Ca, Co, Cr, Cu, Eu, Fe, K, La, Li, Mg, Mn, Mo, Na, Nd, Ni, O, Rb, Ru, Sc, Si, Sm, Sr, Ti, V, Y, Zn, and Zr. These elements can be divided into the following five categories (Buder 2019):

- i)  $\alpha$  elements – Ca, Mg, Si, Ti: created hydrostatically and explosively (depending on the element), by  $\alpha$ -particle capture in massive stars, and released into the ISM by core collapse supernovae (SNe II)
- ii) odd- $Z$  elements – Al, K, Na: produced during supernovae type Ia (SNe Ia) and SNe II, and explosive C, O, and Ne burning
- iii) iron-peak elements – Fe, Co, Cr, Cu, Mn, Ni, Sc, V, Zn: produced during supernovae
- iv)  $s$ -process elements – Ba, La, Rb, Sr, Y, Zr: produced by neutron-capture and decay processes, most likely in AGB stars or massive star winds
- v)  $r$ -process elements – Ce, Eu, Nd, Ru: produced by neutron-capture and decay processes, hypothesized to form during kilonovae

For this analysis, we only use stars with good quality flags for a given element (`flag` = 0), which reduces the Li-rich sample of 1155 stars by less than 15% for most elements, 15 – 50% for Eu, La, Nd, V, Zn, and Zr, by  $\sim 70\%$  for Sm, and by more than 90% for Mo, Rb, Ru, and Sr. Figure 11 shows histograms of the Li-rich and Li-normal populations for each element, with the mean and confidence on the mean ( $\sigma/\sqrt{N}$ ) also reported in each sub-panel. By inspection of the histograms and summary statistics, namely the mean and  $1-\sigma$  standard deviation, the Li-rich and Li-normal samples are near-identical for many elements. In fact,  $\sim 20\%$  of elements have the same mean and  $1-\sigma$  standard deviation within uncertainties, for the Li-rich and Li-normal populations. Within the  $2-\sigma$  uncertainty on the mean,  $\sim 50\%$  of elements<sup>4</sup> have the same mean values in the Li-rich and Li-normal samples. It is perhaps not surprising that most of the supernovae Ia and II element distributions are the same within uncertainties, as  $[\text{Fe}/\text{H}]$  and  $[\text{Mg}/\text{Fe}]$  serve as the doppelgänger criteria. For other elements<sup>5</sup>, we see differences in the mean of the abundance distributions that marginally exceed the error on the mean. However, overall these are still extremely small, and all are below 0.05 dex. Note this difference is lower than the typical precision on these elements in individual stars.

We reorganize the information in Figure 11, and show in Figure 12 the average difference in each abundance, sorted in amplitude along the x-axis. While Figure 11 includes all stars with reported abundances, where the

<sup>4</sup>  $[\alpha/\text{Fe}]$ ,  $[\text{Al}/\text{Fe}]$ ,  $[\text{Ca}/\text{Fe}]$ ,  $[\text{Co}/\text{Fe}]$ ,  $[\text{Cu}/\text{Fe}]$ ,  $[\text{Fe}/\text{H}]$ ,  $[\text{Mg}/\text{Fe}]$ ,  $[\text{Mn}/\text{Fe}]$ ,  $[\text{Mo}/\text{Fe}]$ ,  $[\text{Rb}/\text{Fe}]$ ,  $[\text{Ru}/\text{Fe}]$ ,  $[\text{Sm}/\text{Fe}]$ ,  $[\text{Sr}/\text{Fe}]$ ,  $[\text{V}/\text{Fe}]$

<sup>5</sup>  $[\text{Ba}/\text{Fe}]$ ,  $[\text{Cr}/\text{Fe}]$ ,  $[\text{Eu}/\text{Fe}]$ ,  $[\text{K}/\text{Fe}]$ ,  $[\text{La}/\text{Fe}]$ ,  $[\text{Na}/\text{Fe}]$ ,  $[\text{Nd}/\text{Fe}]$ ,  $[\text{Ni}/\text{Fe}]$ ,  $[\text{O}/\text{Fe}]$ ,  $[\text{Sc}/\text{Fe}]$ ,  $[\text{Si}/\text{Fe}]$ ,  $[\text{Ti}/\text{Fe}]$ ,  $[\text{Y}/\text{Fe}]$ ,  $[\text{Zn}/\text{Fe}]$ ,  $[\text{Zr}/\text{Fe}]$

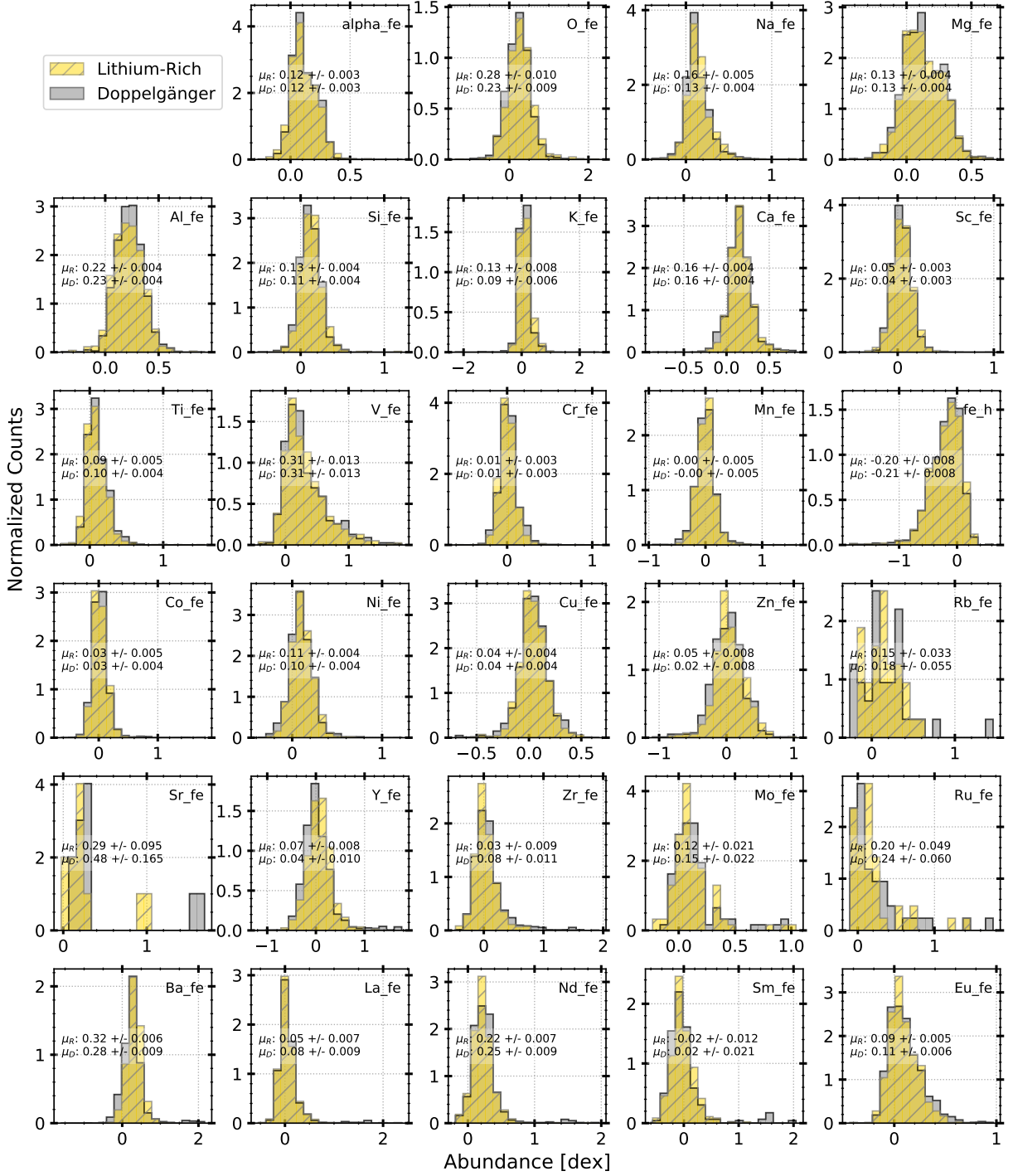


**Figure 11.** Distribution of 30 abundances for the Li-rich (yellow hatched) and Li-normal (grey) sample. The mean abundance and associated error for both samples is indicated in text with  $\mu_R$  and  $\mu_D$ , respectively.

histograms each show on the order of  $\sim 500$  stars, Figure 12, which reports the mean difference in each abundance of the Li-rich star and its doppelgänger, includes  $\sim 15\%$  fewer stars since not all pairs have reported abundances for *both* the Li-rich star and its doppelgänger in each element. Therefore, the mean difference of the pairs may

not be precisely the same as the difference on the means of the histograms in Figure 11, due to the samples being slightly different, and this now being a more robust test of differences in the populations. In Figure 12, we also exclude elements whose distributions were highly non-Gaussian as seen in Figure 11, and those where more

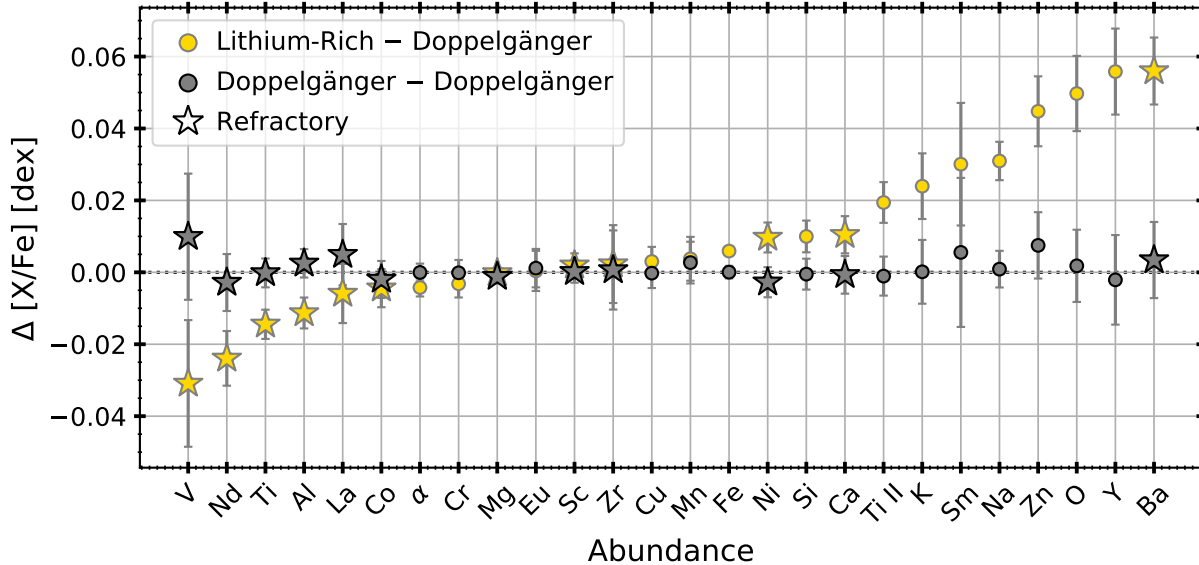


**Figure 12.** Mean difference in abundance between the Li-rich and doppelgänger sample as a function of elements. The star markers indicate the refractory elements, and error bars are shown in grey. The yellow points show the difference between a Li-rich and Li-normal star, and the grey points show the difference between two random doppelgängers of the Li-rich star. Since each point represents the average of 10 samples, the differences between Li-rich and Li-normal sample are more significant compared to differences between the doppelgänger-doppelgänger sample.

than 90% of the sample did not have good quality flags (e.g., Mo, Rb, Ru and Sr).

For Figure 12, we bootstrap the comparison of distributions of each element as follows: for each element abundance measurement and every Li-rich star, we select a doppelgänger at random from the 100 closest doppelgängers, and also select two additional doppelgängers. For every element, we find the mean difference for all stars between the Li-rich and first doppelgänger, as well as the mean difference between two other doppelgängers. We repeat these steps for each element and 10 samples, and use the average of 10 samples – where each sample comprises a comparison of about  $\sim 500$  stars for each element – in Figure 12. For a given element, X, this can be formulated as follows,

$$\Delta[X/\text{Fe}] = \frac{1}{10} \sum_{j=1}^{10} \left( \frac{1}{N} \sum_{n=1}^N X_{n_j} - X_{n'_j} \right) \quad (3)$$

For each element, this gives us a bootstrapped comparison of the abundance distributions of Li-rich stars compared to 10 doppelgänger distributions, and a reference sample of 10 doppelgänger-doppelgänger distributions.

The results are shown on the y-axis of Figure 12, where the yellow points show the mean difference between the Li-rich and Li-normal pairs, and the grey points show the mean difference between pairs of doppelgängers of the Li-rich stars. The error bars represent the

$1-\sigma$  dispersion of the 10 draws. The doppelgänger-doppelgänger difference measurement serves as a reference. The expectation is that these should show zero mean differences, as they are unbiased in being drawn from the same population in  $T_{\text{eff}}$ ,  $\log g$ ,  $[\text{Fe}/\text{H}]$ , and  $[\text{Mg}/\text{Fe}]$ . Conversely, the mean differences in the Li-rich and Li-normal pairs test if the bias in lithium between the pairs is associated with any difference in the individual elements.

We validate that  $[\text{Fe}/\text{H}]$  and  $[\text{Mg}/\text{Fe}]$  have a zero mean difference in the Li-rich and Li-normal pairs, as expected for the two populations, since these parameters define the samples (e.g., see Figure 1 for a summary). About  $\sim 50\%$  of the elements have differences in the Li-rich-Li-normal pairs between 0.01 – 0.06 dex, but for doppelgängers-doppelgängers pairs, all elements show negligible differences, within the sampling uncertainties. The mean overall absolute difference of the doppelgänger-doppelgänger pairs is  $\sim 0.0016 \pm 0.0002$  dex, but that of the Li-rich-doppelgänger pairs is  $\sim 0.0179 \pm 0.0002$  dex, where the errors on these measurements is the inverse weighted variance. The reference test in Figure 12 highlights the significant differences in abundances between Li-rich and Li-normal pairs.

Despite having large samples of stars for each element, there are in some cases reasonably large  $1-\sigma$  standard deviation values of the 10 samples, for the comparisons between the Li-rich-doppelgänger and doppelgänger-

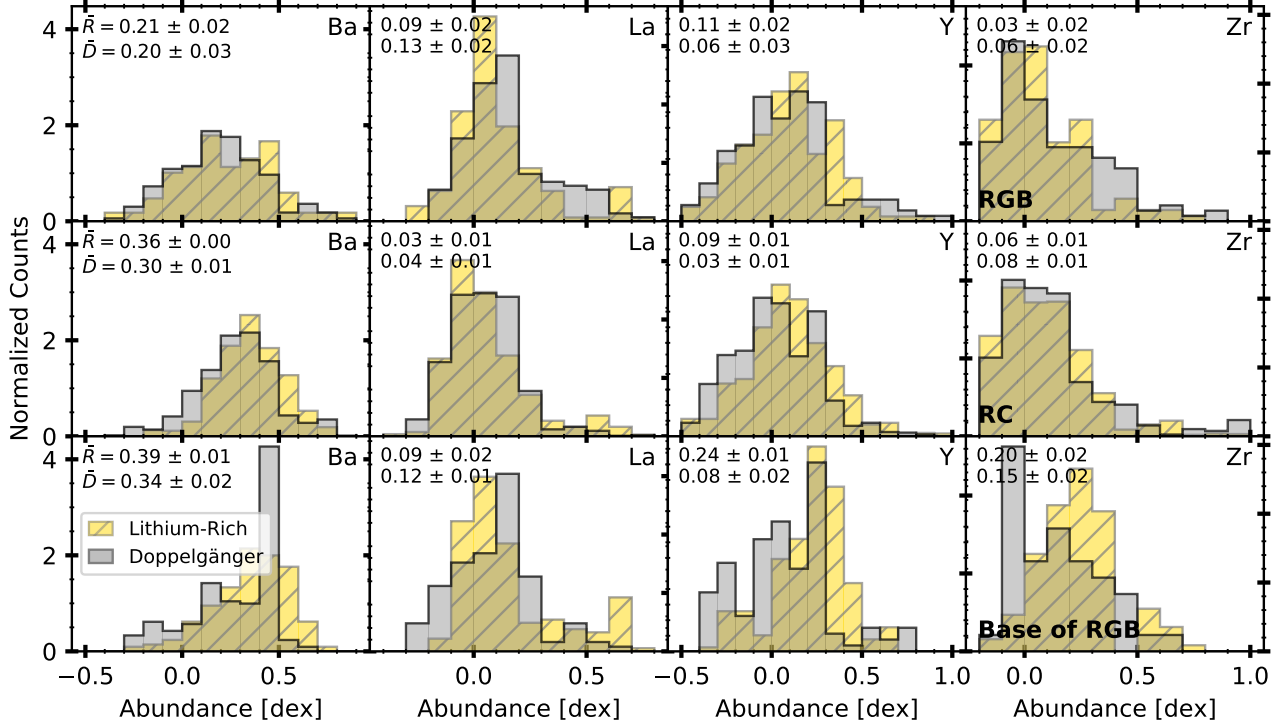


**Figure 13.** Distribution of  $s$ -process elements – Barium (Ba), Lanthanum (La), Yttrium (Y), and Zirconium (Zr) – for stars in three evolutionary states, namely red giant branch (top row), red clump (middle row), and base of the red giant branch (bottom row). The yellow and grey bars indicate Li-rich and doppelgänger stars, respectively, and the text indicates the median abundance for the Li-rich (top) and doppelgänger sample (bottom). There is no significant difference in all four elements for stars in the red giant branch and red clump phases; however, Li-rich stars at the base of RGB have higher amounts of Ba, Y, and Zr, but less La than their doppelgänger. This suggests that stars at the base of RGB are enriched in both lithium and  $s$ -process elements, likely by a companion intermediate-mass AGB star.

doppelgänger distributions (e.g. V, Sm). This implies that there are abundance outliers driven by measurement errors that bias these calculations in some cases, but which we mitigate the effect of with bootstrapping (e.g., as seen in Griffith et al. 2022).

#### 3.4.1. $s$ -process Elements

In our element abundance analysis, we see notable differences in the distribution of  $s$ -process elements. These represent an independent nucleosynthetic channel from our doppelgänger criterion. Differences in the  $s$ -process elements may indicate a role of evolutionary state in the mechanism for Li-enrichment, or else transfer of  $s$ -process material from a binary companion. Stars with anomalously high  $s$ -process enhancements in particular, are proposed to be enhanced via mass-transfer from an AGB binary companion (e.g., Cseh et al. 2018; Norfolk et al. 2019; Cseh et al. 2022; den Hartogh et al. 2022; Escorza & De Rosa 2023).

In Figure 13, we compare the Li-rich and Li-normal distribution of four  $s$ -process elements for three evolutionary states. The RGB and RC phases are defined using the criteria in Martell et al. (2021), and

stars at the base of RGB have  $\log g \geq 2.70$  dex (and less than  $\log g = 3.2$  dex given our sample construction, see Section 3.1). We compare the abundance distributions ( $[X/Fe]$ ) of four elements, from left to right: Ba, La, Y, and Zr (indicated in the top right hand corner of each sub-panel). We notice that Li-rich stars at the base of RGB (bottom row) in particular have slightly higher abundances of  $s$ -process elements compared to their doppelgänger with mean differences exceeding the uncertainties. Yttrium shows the largest difference in the median, with  $\Delta \sim 0.16 \pm 0.02$  dex higher in the Li-rich sample. Therefore, we find that stars at the base of RGB are more likely to be  $s$ -process enhanced.

We further investigate these differences in  $s$ -process elements in Figure 14 where we compare  $[Ba/Fe]$  abundance of the Li-rich and Li-normal samples, coloured by  $T_{\text{eff}}$  of Li-rich stars. We notice a dearth of Ba-rich stars in the Li-rich population that are otherwise present in the doppelgänger population. Highly enhanced barium stars have been recognised in many studies (e.g., Warner 1965; McClure 1984). A possibly important result that we have uncovered is that

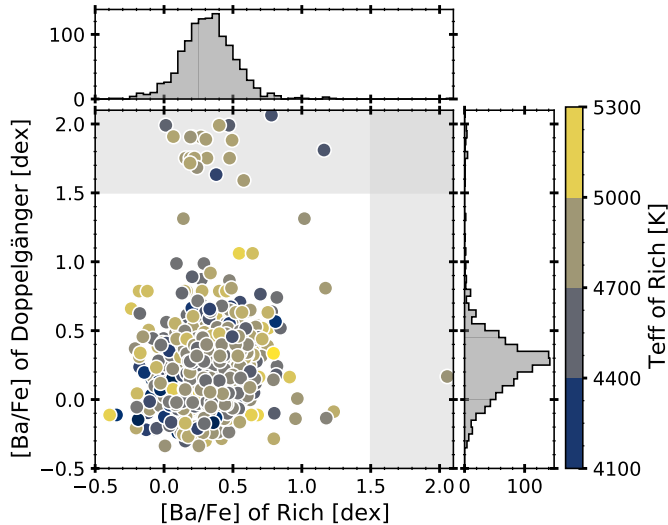


**Figure 14.** Distribution of  $[\text{Ba}/\text{Fe}]$  for Li-rich and Li-normal samples coloured by  $T_{\text{eff}}$  of Li-rich stars. The highly-enriched barium stars that are seen in the doppelgänger are not present in the Li-rich sample. This is evidence that the mechanism by which stars become Ba-rich, likely the mass-transfer of a close low-mass AGB companion, is incompatible with the mechanism for Li-enrichment. Note that two stars fall outside of the axis limits.

the prevalence of these in the Li-rich stars is significantly lower than the field, as seen in Figure 14; the most Ba-enriched stars as seen in the doppelgänger population are in fact entirely missing from the Li-rich sample.

To assign a confidence to the outlier population fraction, we can assume each star represents a Bernoulli trial, so the probability of finding a star with  $[\text{Ba}/\text{Fe}]$  greater than some threshold is given by the binomial distribution (Johnson et al. 2010). Using Bernoulli sampling, we find that only  $0.1\% \pm 0.1\%$  of Li-rich stars have  $[\text{Ba}/\text{Fe}] \geq 1.5$  dex compared to the  $1.8\% \pm 0.4\%$  of doppelgänger. Even using a different threshold of  $[\text{Ba}/\text{Fe}] \geq 1$  dex, we find  $2.3\% \pm 0.4\%$  of doppelgänger compared to  $0.5\% \pm 0.2\%$  of Li-rich stars. This indicates that the mechanism that enriches stars in barium is incompatible with enrichment in lithium.

Note that we see this group of highly-enriched stars for other  $s$ -process elements that are absent from the Li-rich sample (see Figure 19). Therefore, the underlying responsible mechanism behind this is likely associated in general with the  $s$ -process group production. We specifically chose to examine barium since there are more measurements available for barium compared to La, Y, and Zr, and barium measurements have on average the lowest error compared to the others.

### 3.5. Condensation Temperature Trends

We also investigate the chemical abundances of our Li-rich stars and their doppelgänger as a function of condensation temperature. Condensation temperature,  $T_c$ , is the temperature at which 50% of an element condenses from gaseous to solid phase under protoplanetary conditions (Lodders 2003). Analysis of refractory depletion and condensation temperature is widely used to probe dust and rock formation (e.g., Venn & Lambert 1990; Savage & Sembach 1996; Heiter et al. 2002; Maas et al. 2005). Given that rocky planets would form primarily out of high condensation temperature elements, the absence of these elements in the present-day stellar atmospheres has been suggested to arise from a history of planet formation (e.g., Meléndez et al. 2009; Chambers 2010). Alternatively, engulfment of planetary material at late times in the formation process may give rise to enhancements in the abundances of high condensation temperature elements (e.g., Meléndez et al. 2017; Spina et al. 2021). Since this accretion of material would also enhance lithium abundance, we explore this explanation by searching our Li-rich stars for refractory material enhancements (e.g., Ramírez et al. 2009; Gonzalez et al. 2010; Schuler et al. 2011; Ramírez et al. 2011; Meléndez et al. 2012; Liu et al. 2014; Nissen 2015; Schuler et al. 2015; Teske et al. 2016; Bedell et al. 2018; Liu et al. 2020; Nissen et al. 2020).

To look for signatures of planets in our Li-rich stars, we compare  $[\text{X}/\text{H}]^6$  of Li-rich stars and their doppelgänger as a function of condensation temperature for three evolutionary states, namely RGB, RC and base of RGB. We limit the sample by only using stars with a  $\text{SNR} > 50$  in GALAH spectra, and good quality flags for a given element. For all three stages, we found no significant difference trend of  $[\text{X}/\text{H}]$  as a function of condensation temperature. To ascertain that the trend is non-negligible for Li-rich stars, we also analyzed the difference in abundance for two other doppelgänger for each Li-rich star, but found no significant difference between the Li-rich-doppelgänger and doppelgänger-doppelgänger samples.

A positive trend in  $[\text{X}/\text{Fe}]$  as a function of condensation temperature would imply an excess of refractory elements in the Li-rich star, while a negative slope would imply a dearth of refractory elements. Therefore, we calculated the slope from a linear fit on a  $[\text{X}/\text{Fe}] - T_c$  parameter for individual stars. We performed bootstrapping to check if one element had a larger effect on the resulting trend. Removing  $[\text{Na}/\text{Fe}]$  and  $[\text{Sc}/\text{Fe}]$  had the most impact on the slope; however,

<sup>6</sup>  $[\text{X}/\text{H}] = [\text{X}/\text{Fe}] - [\text{Fe}/\text{H}]$

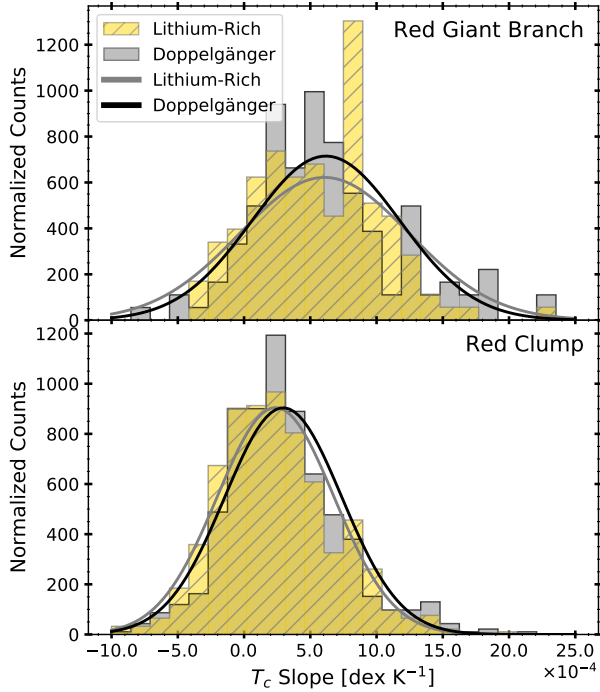


**Figure 15.** Distribution of  $[X/Fe]-T_c$  slope ( $\text{dex K}^{-1}$ ) derived for each Li-rich star (yellow-hatched) and its doppelgänger (grey) plotted for red giant branch (top panel) and red clump stars (bottom panel). Since positive slopes indicate an excess of refractory elements, we see no strong evidence of engulfment events in our Li-rich sample across evolutionary states.

the effect was insignificant and within  $5 - \sigma$  of the mean. Therefore, we fit all elements with a condensation temperature above 1300 K. This condition was chosen given that Bedell et al. (2018) found a bias in the refractory abundance vs.  $T_c$  slopes if volatile elements (ie.  $T_c < 1300$  K) were included.

In Figure 15, we plot the distribution of  $[X/Fe]-T_c$  slopes for RGB (top panel) and RC (bottom panel) stars for both Li-rich stars (yellow) and their doppelgängers (grey), and find a close overlap in the two distributions. Our resulting distributions are similar to those found by Bedell et al. (2018) and Nibauer et al. (2021), and we achieve a similar median to both. Interestingly, we see significantly different slope distributions for the two evolutionary states populations, independently of their lithium abundance. However, the identical distributions in Li-rich and doppelgänger samples seen in Figure 15 suggest no clear role of planet engulfment signature in Li-enrichment mechanism.

#### 4. DISCUSSION

We have four primary results summarized below:

- i) Section 4.1: Li-rich stars are more likely to be red clump rather than red giant branch stars. The increasing prevalence of red clump membership at higher Li-enrichment implies there is an evolutionary state dependence on lithium production, such as one associated with the He-flash.
- ii) Section 4.2: We detect differences in the H- $\alpha$  in a subset of Li-rich stars ( $\sim 20\%$ ), which is twice the incidence of the same signal in the doppelgängers. This could reflect potential differences in rotation, chromospheric activity, and/or binarity between Li-rich stars and their doppelgängers. We also report a faster rotation for a subset of the Li-rich population as measured by the broadening velocity parameter. This difference in the populations of Li-rich and doppelgängers as seen in the spectra and broadening velocity indicates internal enrichment via binarity – as a driver of the Cameron-Fowler mechanism – is responsible for Li-enrichment, for a subset of the population. Whether the line profiles and broadening velocity are due to true differences in rotation, or if they are a direct binary detection, this profile links to the role of a companion for these stars.
- iii) Section 4.3: We discover a dearth of Ba-rich stars in the Li-rich sample, which are present in the Li-normal sample. We therefore conclude that the mechanism for high Ba-enrichment prohibits Li-enrichment for a subset of stars. This result may be due to a population of stars that have had  $s$ -process enhancing  $low$ -mass AGB companions, which are not a source of lithium themselves, but preclude enrichment via planetary engulfment or wide-binary tidal spin-up.
- iv) Sections 4.4: We see some population differences in the abundance distributions of the Li-rich and Li-normal stars which change with evolutionary state, suggesting multiple mechanisms for Li-enrichment. In particular, Li-rich stars show higher  $s$ -process abundances than their doppelgängers at the base of RGB, where internal mechanisms should not be responsible for Li-enrichment. This is a possible signature of mass-transfer from *intermediate*-mass AGB companions, leading to both lithium and  $s$ -process enhancements. The lack of any condensation temperature trends and differences in refractory element abundances indicates no lines of evidence for the role of planetary ingestion.

##### 4.1. Lithium in red clump and red giant branch stars



We find a clear increasing probability of red clump membership as a function of Li-enrichment, in agreement with previous studies (e.g., Casey et al. 2019; Deepak & Reddy 2019; Deepak & Lambert 2021a,b; Martell et al. 2021). Singh et al. (2019) used asteroseismology to determine that most stars in their sample were from the He-core burning phase, similar to results found by Ming-hao et al. (2021). Similarly, Zhou et al. (2022) found that  $\sim 71\%$  of their Li-rich sample belong to the red clump, and concluded that Li-rich are rare in the red giant phase, while Yan et al. (2021) found a ratio of 75% for RC to RGB stars (given  $A(\text{Li}) = 1.5$  dex).

Recent studies suggest a universal lithium production mechanism occurs between the RGB and RC phases, potentially at the He-core flash. This has been proposed using evidence from observations (e.g., Kirby et al. 2012b, 2016; Kumar et al. 2020; Mallick et al. 2023), and expectations from theoretical models (e.g., Schwab 2020; Mori et al. 2021; Magrini et al. 2021). However, Chanamé et al. (2022) strongly argued there is no evidence for a lithium production event on the red clump when the dependency of lithium depletion on stellar mass in standard stellar models is accounted for, and that the results from Kumar et al. (2020) are biased due to sample selection. In fact, Kirby et al. (2012b) attribute the brevity of this ubiquitous lithium production event to the observed low number of Li-rich giants. Our finding of the increasing prevalence of red clump membership for higher Li-enriched stars implies the He-flash induced lithium production is a plausible explanation for these observations.

#### 4.2. Signatures of possible binarity

In analyzing spectra of Li-rich stars and their doppelgängers, stars selected to have the same stellar parameters ( $T_{\text{eff}}$ ,  $\log g$ ,  $[\text{Fe}/\text{H}]$ ,  $[\text{Mg}/\text{Fe}]$ ) show similar, but non-identical spectra, where the most significant deviations are in the H- $\alpha$  feature (see Figure 4). We classified the differences at the H- $\alpha$  feature between Li-rich and doppelgängers into *W* and *M* profiles, and found  $\sim 20\%$  of the Li-rich population to have a *W*-designation compared to  $\sim 10\%$  of the doppelgängers. Section 4.2.1 shows that this profile is consistent with one of the stars in the pair being in a (spectroscopic) binary system. If all profiles directly tag (in effect, spectroscopic) binaries, this means the Li-rich stars have twice the binary fraction of the reference population of doppelgängers for these architectures. Furthermore, because of the advancements of *Gaia* (E)DR3 over *Gaia* DR2, it is possible that previously unresolved binaries with one

source identifier in *Gaia* DR2 are now resolved in *Gaia* DR3 with two source identifiers (Torra et al. 2021). Comparing the percentage of changed source identifiers between Li-rich and Li-normal stars can therefore yield another hint of binarity. We find that 6.4% (93/1455) of the Li-rich giants have new *Gaia* DR3 source identifiers, whereas only 2.7% (207/7543) of the Li-normal giants have new *Gaia* DR3 source identifiers.

We investigate the velocity broadening parameter ( $v_{\text{broad}}$ ), as measured from the spectra. This confirms that the subset of Li-rich stars with H- $\alpha$  profiles that are indicative of faster rotation than their doppelgängers (*W*-designations) have preferentially higher broadening velocity than those with slower rotation than their doppelgängers (*M*-designations). This could be a true velocity broadening or simply due to the system being a binary and not single star. Nevertheless, this also showcases the differences in the Li-rich and doppelgänger population.

As seen in Figure 7, there is a marked higher occurrence of stars with larger  $v_{\text{broad}}$  ( $\gtrsim 20 \text{ km s}^{-1}$ ) for stars with  $A(\text{Li})$  between 1.5 – 2.7 dex, which is larger than the expected average  $v_{\text{broad}}$  ( $\sim 10 \text{ km s}^{-1}$ ) for red giants (e.g., Carney et al. 2008; Patton et al. 2023). Stars above this lithium threshold extend beyond  $20 \text{ km s}^{-1}$ , but a subset extend to  $\sim 50 \text{ km s}^{-1}$  below it. Figure 7 suggests there are likely multiple architectures leading to Li-rich and super Li-rich stars. The lesser Li-rich stars appear to comprise the subset of the fastest rotators, while very few of the more enhanced stars are measured to be rotating faster than their doppelgänger. This may be linked to the close binary fraction and detection limits of different types of spectroscopic binaries.

The differences in the line profiles that we see in the H- $\alpha$  and Ca-triplet features could also be produced by differences in the magnetic activity levels on Li-rich and doppelgängers stars. Kowkabay et al. (2022) found variable emission in the wings of the H- $\alpha$  absorption line in the multi-epoch spectra of a recently discovered ultra Li-rich metal-poor star. The authors associate this with a mass-loss event and possible outflows. An excess of magnetic activity is expected in both the presence of a binary companion (e.g., Montes et al. 1996; Sahai et al. 2008) as well as planetary engulfment, since binary companions would lead to enhanced rotation in particular configurations due to tidal interactions which spin-up the primary (Casey et al. 2019). Therefore, it would be prudent to follow up the GALAH Li-rich targets similarly, with multi-epoch photometry and spectra, and/or radial velocity measurements from other surveys. This would test the role of binarity, rotation,

and variability in the magnetic activity of the Li-rich sample over time.

In summary, the line profile and broadening velocity parameter results are clear lines of evidence for the role of binaries leading to Li-rich giants. Binary systems are the main prediction for triggering the internal Cameron-Fowler mechanism of Li-enrichment. In this scenario, the primary in a binary system is tidally spun-up from the companion, which is proposed to induce this internal lithium production process (Casey et al. 2019).

A particularly interesting and telling result that we uncover is the marginal differences in the mean abundances for some elements between Li-rich stars and their doppelgänger. In particular, we see differences between the  $s$ -process abundances at the base of RGB, where the Li-rich stars show higher  $s$ -process elements than their doppelgänger (see Figure 13). We note that these differences are small,  $\leq 0.05$  dex, with the exception of  $[Y/Fe]$  which shows a mean difference of 0.16 dex. Unlike along the RGB, any element abundance differences at base of RGB are unlikely to come from internal source (Aguilera-Gómez et al. 2016b), and therefore suggest an external mechanism of enrichment for these stars. These observations may be explained by intermediate-mass AGB companions ( $\gtrsim 4 - 8 M_{\odot}$ ; Uttenthaler et al. 2007).

Intermediate-mass AGB stars are theorized to make lithium in their envelopes via the process of ‘Hot Bottom Burning’ (HBB; Sackmann & Boothroyd 1992). When the bottom of the convective layer reaches 40 MK, non-negligible nucleosynthesis can take place when the bottom of the convective layer merges with the outer hydrogen burning layers. HBB has been attributed to produce large amounts of lithium found in the surfaces of evolved stars, especially those with a high lithium abundance ( $A(\text{Li}) \sim 4.5$  dex). If an AGB and RGB star are in a binary system and the AGB is Li-enhanced, then the AGB star could transfer some of its Li-enriched material to the red giant creating a super Li-rich red giant. Since AGB stars are enriched in  $s$ -process elements, we would expect the red giant to also be similarly enriched (Smith & Lambert 1989). This is discussed in more detail in Section 4.3.

Regardless, if the Li-rich stars underwent a planetary engulfment event, accreted material from an AGB, or experienced rapid rotation caused by interaction with a binary or via tidal spin-up, we might expect to see an effect on chromospheric activity (e.g., Metzger et al. 2012). Therefore, we looked for emission in the UV using GALEX data and emission in the IR using WISE, but found no differences between the Li-rich and Li-normal populations in the two bands. Many studies

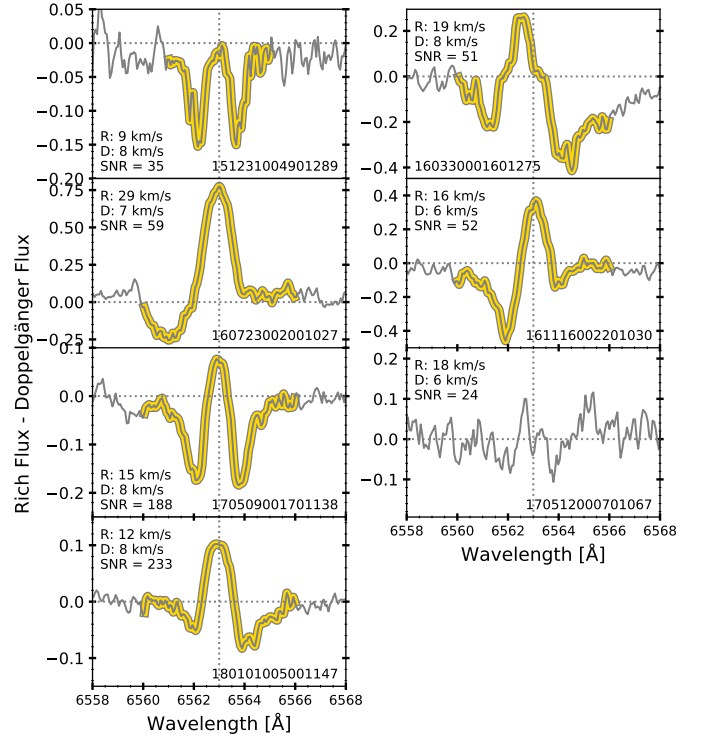


**Figure 16.** Difference in flux for 7 Li-rich stars flagged as line-splitting binaries in GALAH, centered on the H- $\alpha$  line. The yellow curve highlights the  $W$ -profile, and the text includes the  $v_{\text{broad}}$  for both the Li-rich star and its doppelgänger, and the signal-to-noise of the Li-rich spectrum in GALAH.

have already utilized GALEX to probe stellar activity (e.g., Findeisen et al. 2011; Shkolnik et al. 2011; Stelzer et al. 2016; Dixon et al. 2020). However, we see no such UV excess for Li-rich stars (see Figure 10). Finding no evidence of IR and UV emission could be due to observational bias, since only the brightest red giants would show high UV emission. In fact, Findeisen et al. (2011) found little correlation between near-UV emission and activity for stars older than  $\sim 0.5 - 1$  Gyr. Similarly, IR excess is mostly expected for young stellar objects.

#### 4.2.1. Binarity flags in GALAH

During our sample construction, we require that all stars in GALAH have  $\text{flag\_sp} \leq 1$ , which GALAH attributes to objects if no problems were identified in determination of their stellar parameters. However, GALAH also flags line-splitting binaries, which we excluded in the original sample, when imposing the condition  $\text{flag\_sp} \leq 1$ . Therefore to probe binarity, we now specifically analyzed these excluded, flagged stars. A  $\text{flag\_sp} = 32$  is given to a star by GALAH if its spectrum looks similar to a line-splitting binary

spectrum as found by a spectrum comparison algorithm (“tSNE”). Incorporating this condition results in 7 new Li-rich stars, but no Li-normal stars. For the 7 new Li-rich star, we find a doppelgänger using the method described in Section 2.2, but without requiring that the difference in stellar parameters be less than the error on said parameter; this is justified since stellar parameters and abundances can be inaccurate for binaries.

In Figure 16, we plot the difference in flux for the 7 new Li-rich stars and their doppelgängers, centered on the H- $\alpha$  line, and include the  $v_{\text{broad}}$  for both stars. We notice that 6 of the 7 Li-rich stars produce a  $W$ -profile with respect to their doppelgänger, and even see a tentative  $W$ -profile in the seventh star, possibly less apparent due to the SNR of the Li-rich spectrum, which is only 24. We also find that  $v_{\text{broad}}$  for the majority (5/7) of Li-rich stars in Figure 16 is twice as large.

The amplitude of these profile differences is extremely high in some cases, much higher than the  $\sim 10\%$  level we detect in Figure 5. However, this clearly demonstrates that what we may be detecting with our  $W$  and  $M$  profiles is binary systems. In the case of the Li-rich star being in the binary, the profile of the difference is the  $W$  shape and when it is the doppelgänger, it is the  $M$ . Subsequently, some of the enhanced rotation that is being measured and documented in Section 3.3.1, by the broadening velocity, may in fact be due to binarity being captured by this parameter. Therefore, we may have created, via the doppelgänger reference comparison, a highly sensitive method to detect spectroscopic binaries that are otherwise evading detection. These stars will not be flagged binaries with the RUWE parameter, which is instead preferentially sensitive to wide separation binaries (discussed in detail in Section 4.2.3). Indeed, the 6 of the 7 stars shown in Figure 16 all have  $\text{RUWE} < 1.2$ . However, these stars would presumably show radial velocity variations over time detectable in multi-epoch survey data. We intend to follow up the stars that we have flagged as either  $W$  and  $M$  with complementary survey data to verify what fraction of these are indeed in binary systems.

#### 4.2.2. Expected parameter space of potential binary systems

Although RUWE values derived in *Gaia* can be used to identify binary architectures, we can also predict the separations and mass ratios that would likely produce the observed RUWE values in our sample. An unresolved binary would cause a single-source astrometric model to perform poorly, resulting in a high  $\chi^2$ ; this is equivalent to RUWE or  $\rho$ , the re-normalised unit weight error. We derive  $\rho$  for stars with orbital separations between 0 – 10 AU, and mass ratios

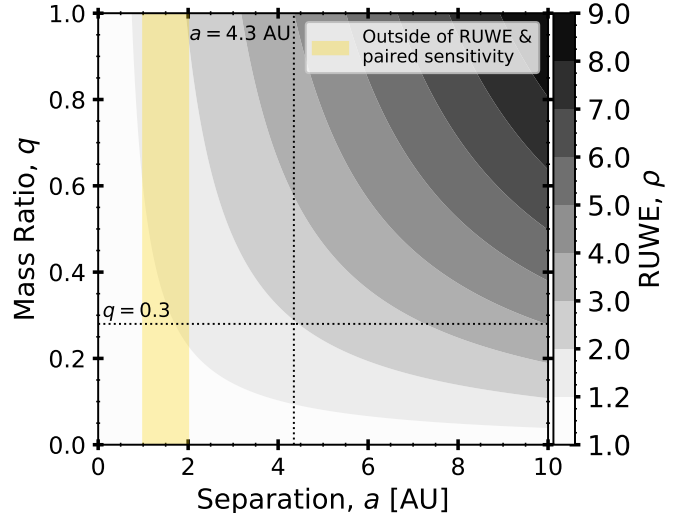


**Figure 17.** Expected RUWE values for a binary system given a range of orbital separations and mass ratios. Given the observed RUWE values, we can eliminate regions of this parameter space where  $\text{RUWE} \gtrsim 4$ . The dashed lines are shown as reference for relevant boundaries of the mass ratio and separation.

between 0 to 1. We briefly outline the steps below, and direct the reader to Belokurov et al. (2020) for a more detail description of the methods. We calculate  $\rho$  using the following,

$$\delta\theta = \sqrt{\langle \delta\theta_i^2 \rangle} \approx \sigma_{\text{AL}}(G)\sqrt{\rho^2 - 1} \quad (4)$$

$$\frac{\delta a}{\text{AU}} = \frac{\delta\theta}{\text{mas}} \frac{D}{\text{kpc}} \quad (5)$$

$$\delta a \propto \frac{a|q - l|}{(q + 1)(l + 1)} \quad (6)$$

given a mass ratio  $q = m_2/m_1$ , luminosity ratio  $l = l_2/l_1$ , angular perturbation  $\delta\theta$ , wobble  $\delta a$ , and distance to source  $D$ . We assume  $l = 0$  since we cannot see the secondary companion for our stars, and  $D = 2.2$  kpc which is the mean distance for our sample. Given a  $G$  magnitude, we use Figure 9 in Lindegren et al. (2018) to approximate  $\sigma_{\text{AL}}$ , the per-scan along-scan centroiding error. The mean  $G$  magnitude of our stars is 12.2 which results in  $\sigma_{\text{AL}} = 0.25$ .

In Figure 17, we show the predicted RUWE for a range of orbital separations and mass ratios. As expected, the largest RUWE is seen at the largest mass ratio, since the higher the mass of the faint object, the more the wobble of the bright object ( $l_1, m_1$ ). Similarly, RUWE is higher for large separations since the wobble produced by the star on the sky is larger. For the range of RUWE values in our sample, which is 0.6 – 4, the

**Table 3.** Analysis with `paired` for Li-rich stars and their doppelgängers. Stars with a RUWE  $\geq 1.2$  are predicted to be contaminated by a close companion, while stars with  $p$ -value  $\leq 0.001$  are flagged as potential binaries in `paired`.

	Li-rich		Doppelgänger	
Total	1155	–	830	–
In <code>paired</code>	1128/1155	(98%)	803/830	(97%)
RUWE $< 1.2$	1055/1128	(94%)	753/803	(94%)
RUWE $\geq 1.2$	73/1128	(7%)	50/803	(6%)
$p$ -val $\leq 0.001$	68/1128	(6%)	58/803	(7%)
RUWE $< 1.2$ & $p$ -val $\leq 0.001$	57/1055	(5%)	52/753	(7%)
RUWE $\geq 1.2$ & $p$ -val $\leq 0.001$	11/73	(15%)	6/50	(12%)

parameter space that covers these RUWE values are, for the majority, stars at close separations, of  $a \sim 0 - 6$  AU, for a range of mass ratios between companions. We exclude the presence of any binaries along the darkest coloured contours, i.e. at separations  $\gtrsim 7$  AU at mass fractions  $\gtrsim 0.5$ . If the Li-rich stars are in binaries, the RUWE values demonstrate that these would be close enough for past mass-transfer between the primary and an AGB companion, where a mass-transfer event could enhance the primary in lithium and other elements (i.e.  $s$ -process elements).

#### 4.2.3. Evidence of binarity with `paired`

To search for more direct evidence of stellar multiplicity, we used `paired`, a statistical framework that uses *Gaia* radial velocity error measurements to search for binarity (Chance et al. 2022), which typically detects binaries at separations of up to a few AU and mass ratios above 0.1. Stellar multiplicity can be detected in the *Gaia* radial velocity measurements as the presence of excess noise, compared to stars of similar apparent magnitude and colour. With proper calibration of the expected radial velocity jitter for similar sources, one can estimate a probability that a source is a non-single star based on its reported radial velocity error in *Gaia*, and the number of radial velocity transits.

We analyzed the `paired` probability for our sample in combination with RUWE which is sensitive to close binaries, where stars with RUWE  $\geq 1.2$  are likely to be binaries (e.g., Berger et al. 2020). For both the Li-rich and Li-normal samples, we compare the number of binaries based on the RUWE and `paired` criteria, where a  $p$ -value  $\leq 0.001$  is flagged as a potential binary in `paired`. Table 3 shows the results of this comparison.

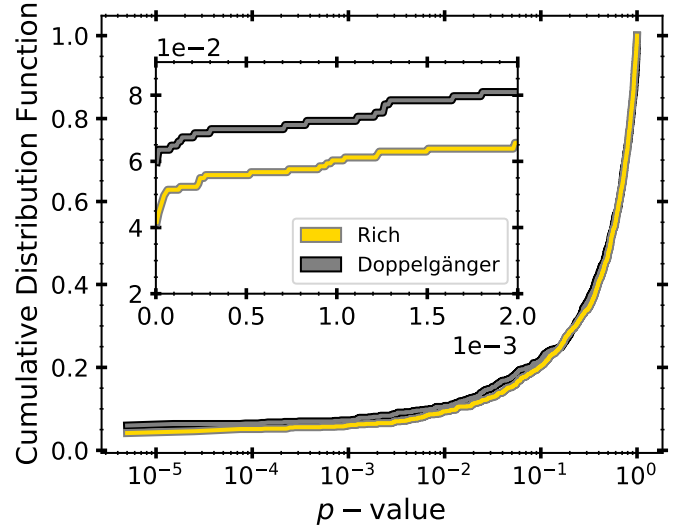


**Figure 18.** Cumulative distribution function (CDF) of  $p$ -value of Li-rich and Li-normal stars in `paired` catalog where both the Li-rich star and its doppelgänger have a  $p$ -value available. The value of CDF at  $p$ -value = 0.001 corresponds to stars flagged as binaries. The CDF of the two samples is similar which suggests that either the Li-rich in binaries have larger separations than the method is sensitive to detect ( $>$  a few AU), or another mechanism causes Li-enrichment for these stars. The inset plot shows the zoomed-in distribution around  $p$ -value = 0.001.

Of the Li-rich stars that have a RUWE  $\geq 1.2$ , only 15% (11/73) are classified as binaries based on RUWE and `paired`. In contrast, of the doppelgängers with a RUWE  $\geq 1.2$ , 12% (6/50) are possible binaries. These low fractions are in agreement with Figure 17 that demonstrates that RUWE  $\geq 1.2$  arises from systems with  $a \geq 2$  AU, which `paired` is not sensitive to. For stars with RUWE  $< 1.2$ , which corresponds to the majority of our sample, 5% (57/1055) of the Li-rich are binary detections in `paired` compared to 7% (52/753) of the doppelgängers.

We suspect that  $W$ -designated Li-rich stars and the  $M$ -designated doppelgänger stars are in binary systems, that have relatively close separations ( $\lesssim 2$  AU, see Figure 17) and are up to near-equal mass (from the line difference profiles, see Figure 5). Therefore, we compared `paired` classification for the Li-rich stars with  $W$  and  $M$  designations. Only 2% (2/83<sup>7</sup>) of the  $M$ -designated Li-rich stars would be classified as a binary based on their radial velocity error; this compares to 13% (27/213) of the  $W$ -designated Li-

<sup>7</sup> This number is smaller since not all  $M$ - and  $W$ -designations were found in `paired`.

rich stars. Therefore, *W*-designated Li-rich stars are substantially more likely to be binaries according to **paired**, compared to *M*-designated stars (where the doppelgänger would be the potential binary). This provides clear evidence to associate the *W* and *M* profiles with binary architectures. Note that only a fraction,  $\sim 15\%$ , of the *W* and *M* profiles are firm binary candidates; therefore, it is possible that these systems include separations that lie in between the **paired** and RUWE sensitivity range ( $\sim 1 - 2$  AU).

We also examined the **paired** binary fraction as a function of evolutionary state for the Li-rich and Li-normal samples. Of the 124 Li-rich RGB stars, 15% are classified as binaries in **paired** compared to 5% of the Li-rich RC stars. Similarly, of the 135 Li-normal RGB stars, 11% are classified as binaries, compared to 5% of the Li-normal RC stars. Given the similar fractions, the two populations are the same in terms of binary architectures detected via RUWE and **paired**.

In Figure 18, we show the cumulative distribution function of *p*-values for Li-rich stars and their doppelgängers. The distributions are marginally different at the threshold value of *p*-value  $\leq 0.001$ : the Li-rich stars reach 6% compared to 7% for the doppelgängers. This implies that the selection function of GALAH renders the recovery rate of binaries very small.

In summary, the RUWE analysis rules out systems with mass ratios above 0.5 at separations of 7 AU, or mass ratios of  $\sim 1$  at separations of 5 AU, while **paired** is sensitive to separations  $< 1$  AU. We can see from Figure 17 that any binary systems with RUWE  $< 1.2$  will be restricted to systems with separations of  $\lesssim 2$  AU for equal mass binaries, and  $\lesssim 3$  AU for binary mass ratios of  $\sim 0.4$ . The **paired** analysis shows the *W* and *M* designations in the spectra comparisons are associated with binarity, and that there is a higher overall binary fraction for the Li-rich population compared to the Li-normal. However, the binary detection rate is extremely low overall.

#### 4.3. Dearth of Barium-rich stars that are Lithium-rich

We found a surprising result where a subset of Ba-rich stars that are seen in the doppelgänger population are not present in the Li-rich sample. This is shown in Figure 14 where we see a small population of stars in the doppelgänger sample with high barium. We note that  $\sim 1.9\%$  of doppelgängers are very enhanced in [Ba/Fe] (ie. [Ba/Fe]  $\geq 1.5$ ) as compared to only  $\sim 0.1\%$  of Li-rich stars. Moreover, Li-normal stars with high [Ba/Fe] have low [Fe/H], supporting previous studies (Karakas et al. 2014; Kirby et al. 2016).

Highly Ba-rich stars are believed to have been recipients of *s*-process material from an AGB companion, via mass-transfer as the secondary overflows its Roche lobe (e.g., Stancliffe 2021; Cseh et al. 2022; Norfolk et al. 2019). Statistically, studies have shown that barium stars are found in binary systems (e.g., McClure et al. 1980; McClure 1983; Jorissen & Mayor 1988; McClure & Woodsworth 1990; Jorissen et al. 1998; Hansen et al. 2016), where the secondary would now be a white-dwarf in our observed systems. This result can be explained by a close (within a few AU) low-mass ( $\lesssim 4 M_{\odot}$ ) AGB companion, that precludes mechanisms of Li-enrichment, both from planets and from tidal spin-up from a wider binary, as well as the AGB material itself.

Unlike higher mass AGB stars, the lower mass range of the AGB does not produce lithium in HBB (Ventura et al. 2020). Thermohaline mixing has been proposed as a possible alternative route via which low-mass AGB stars can produce lithium (Cantiello & Langer 2010). However, this result indicates that this mechanism must be inefficient, or short lived, as these highly enriched barium stars are not correspondingly Li-rich. Thus, a star can not become Li-rich when extremely Ba-rich. This result combined with the binarity analysis means that the tidal spin up induced Cameron-Fowler mechanism may be limited by specific binary configurations, and this particular channel is limited to low-mass binaries at large radial separations.

#### 4.4. Sub-stellar object engulfment as a mode of enrichment on the RGB

Accretion of a planet or brown dwarf is expected to raise abundances of surface elements, including lithium (e.g., Koch et al. 2011, 2012). Siess & Livio (1999a,b) were the first to explore the planetary engulfment scenario as a possible mechanism for Li-enhancement, but many studies have suggested planetary engulfment as a possibility for Li-enhancement (e.g., Adamów et al. 2012; Aguilera-Gómez et al. 2016b,a). However, while some place an upper limit on the mass of the engulfed object that could produce an observable signature in the star (e.g.,  $15 M_J$  in Aguilera-Gómez et al. 2016b), others suggest no connection between lithium and the presence of planets (e.g., Baumann et al. 2010).

Indeed if planetary engulfment were the mechanism for a significant fraction of Li-rich RGB stars, then we might see an excess in refractory elements for these targets, as well as trends in condensation temperature that differ between Li-rich and Li-normal stars. Motivated by this idea, we derived the [X/Fe]- $T_c$  slope for all stars in our Li-rich and doppelgänger samples (see Figure 15), but found no difference in

measurements between the two samples, nor an excess in refractory elements across evolutionary states; we therefore find no evidence for planetary engulfment in our study. Despite our null results, we do not believe planetary engulfment should be excluded as a possible mechanism for Li-enrichment for two reasons.

Firstly, previous studies that compared condensation temperature and chemical abundances in planet hosts are inconsistent in their findings, and there is a lack of consensus on whether condensation temperature is an appropriate indicator for the presence of planet formation itself. For instance, [Ramírez et al. \(2011\)](#) and [Tucci Maia et al. \(2014\)](#) studied the chemical composition as a function of condensation temperature in 16 Cygni where 16 Cyg B is a planet host. They find no trend between abundance differences and condensation temperature, nor any correlation between condensation temperature and the planet host star. This is in agreement with other similar studies (e.g., [Liu et al. 2014](#); [Teske et al. 2016](#); [Liu et al. 2020](#); [Deepak et al. 2020](#); [Nissen 2015](#)). On the contrary, some studies find promising results in this parameter space. For instance, [Meléndez et al. \(2009\)](#) found that the Sun is more depleted in refractory elements as compared to solar-twins, with others producing similar results (e.g., [Ramírez et al. 2009](#); [Gonzalez et al. 2010](#)). Interestingly, some studies even found contradicting results in their own sample ([Schuler et al. 2011, 2015](#)).

Secondly, we must also consider timescales involved with planetary engulfment, such as lithium survival and planet inspiral timescales. Red giants are expected to remain Li-rich for  $\sim 2$  Myr ([Casey et al. 2019](#)), and even significant signatures from planetary engulfment would have a maximum Li-7 survival time of  $0.5 - 0.9$  Gyr ([Soares-Furtado et al. 2021](#)). However, [Behmard et al. \(2022a\)](#) reported that planetary engulfment signatures are short lived,  $\sim 90$  Myr for  $\sim 1 M_{\odot}$  star, and that these signatures would no longer be observable  $\sim 2$  Gyr after engulfment. Considering that our Li-rich stars range from  $0.4 - 11.2$  Gyr old, where RGB stars are  $\sim 1 - 11$  Gyr old, it may be difficult to observe the evidence of any engulfment in our sample, since engulfment signatures are difficult to see for older stars ([Behmard et al. 2022a,b](#)).

Assuming planetary engulfment were the sole mechanism for Li-enrichment, we can calculate the approximate expected number of Li-rich RGB stars. From analysis done by [Soares-Furtado et al. \(2021\)](#), signatures of engulfment are diluted at later stages of post main-sequence evolution, with abundance measurements falling below 1.5 dex. Therefore, to observe lithium enrichment signature with statistical

**Table 4.** Quantitative summary of main results.

Measurement	Li-rich	Doppelgänger
$\text{RUWE} \geq 1.2$ ( $\gtrsim 2$ AU separation binaries)	7%	6%
$p\text{-val} \leq 0.001$ ( $\lesssim 1$ AU separation binaries)	6%	7%
Spectroscopic binary flag set in GALAH	7 stars	0 stars
$W$ -designation in H- $\alpha$	19%	8%
$v_{\text{broad}} \geq 20 \text{ km s}^{-1}$	2%	1%
Renamed sources between <i>Gaia</i> DR2 & DR3	6%	3%
X/H vs. $T_c$ slope ( $\times 10^{-4}$ ) [dex/K]		
– Red giant branch	$5.8 \pm 0.6$	$5.5 \pm 0.5$
– Red clump	$1.9 \pm 0.2$	$2.6 \pm 0.2$
Results for Li-rich sample only		
Red clump fraction (Li-rich:background)		
$A(\text{Li}) = 1.5 - 1.8$ dex		1.4
$A(\text{Li}) = 2.8 - 4.2$ dex		2.2
Mean elemental abundances relative to doppelgängers		
$\Delta(\text{Ba})$		$0.06 \pm 0.01$
$\Delta(\text{Y})$		$0.06 \pm 0.01$
$\Delta(\text{O})$		$0.05 \pm 0.01$
$\Delta(\text{Zn})$		$0.04 \pm 0.01$
$\Delta(\text{Na})$		$0.03 \pm 0.01$
Mean elemental abundances at the base of RGB		
Ba		$0.39 \pm 0.01$
Y		$0.24 \pm 0.01$
Zr		$0.20 \pm 0.02$

significance, the host star should have a mass of  $1.4 - 1.6 M_{\odot}$ , with the strongest signature occurring for stars with mass above  $1.4 M_{\odot}$ . Of the 449,553 RGB stars in GALAH, 21,113 have a stellar mass between  $1.4 - 1.6 M_{\odot}$ ; therefore, we would expect  $\sim 211$  Li-rich RGB stars, assuming the engulfed planet is a hot Jupiter and  $\sim 1\%$  of giants are expected to host these planets. In principle, all 134 RGB stars in our Li-rich sample could be explained by planetary or brown dwarf engulfment, but realistically we expect only a fraction of Li-rich RGB stars to have undergone planetary engulfment (e.g., [Casey et al. 2019](#); [Soares-Furtado et al. 2021](#)).

## 5. CONCLUSION

We have undertaken a thorough analysis, with the aim to determine the formation mechanisms of Li-rich giants, using new available data from GALAH, and complementary data from *Gaia* DR3 and GALEX. We assembled a sample of 1155 Li-rich stars in GALAH, and compared it to a sample of otherwise identical Li-normal star. Our main conclusions are as follows, quantitatively summarized in Table 4:

- a) Figures 11, 12, 13, 14: inspection of  $s$ -process elements at varying evolutionary states suggests mass-transfer from either low-mass or

- intermediate-mass AGB companions. In addition, we notice a dearth of Ba-rich stars in our sample of Li-rich stars which are present in the population of doppelgängers. These two findings suggest that for stars at the base of RGB, mass-transfer from an *intermediate*-mass AGB leads to enrichment in both lithium and *s*-process elements, while for another subset, mass-transfer from a *low*-mass AGB causes enrichment in *s*-process elements, but prohibits Li-enrichment. The presumably low-mass AGB companion can not be enriched in lithium for any significant period of time, and precludes any enrichment from planetary or brown dwarf engulfment, nor internally induced production from tidal spin-up from a wider binary.
- b) Figures 16, 17, 18: examination of radial velocity error in *Gaia* in combination with simulated RUWE values suggests that binarity could be responsible for a subset of Li-rich stars. This mechanism is likely initiated over a limited range of orbital parameters. The RUWE measurement excludes systems with mass ratios  $\gtrsim 0.5$  at separations  $\gtrsim 7$  AU. Conversely, **paired** is only sensitive to binary separations of  $< 1$  AU, and confirms that *W*-designated Li-rich stars are preferentially binaries. The corresponding RUWE for these stars in combination with the **paired** detection restricts their parameter space to separations of  $\sim 1 - 2$  AU for equal mass binaries, and up to 1 AU for mass ratios of 0.5. These would allude detection as binaries in both **paired** and RUWE, but may be showing up in the spectra in the two-fold incidence of *W*-profiles compared to *M*-profiles. Furthermore, stars flagged as line-splitting binaries in GALAH are exclusively Li-rich, and not Li-normal. These stars are 6/7 times classified as *W*-profiles, and have higher  $v_{\text{broad}}$  compared to their doppelgängers. This strongly suggests that *W* and *M* profiles are spectroscopic binaries at restricted separations.
- c) Figures 4, 5, 7, 8, 9: differential analysis of GALAH spectra show that a subset of Li-rich stars are rotating faster than their Li-normal counterparts. This may be intrinsic rotation or the impact of binary systems on this parameter. We find twice as many anomalously high rotators ( $v_{\text{broad}} \gtrsim 20 \text{ km s}^{-1}$ ) in the Li-rich sample compared to the doppelgänger population. Higher broadening velocities are seen for stars below  $A(\text{Li}) = 2.7$  dex. The changing distribution of broadening velocities and *W*-designations for the Li-rich population as

a function of lithium implies multiple mechanisms of enrichment.

- d) Figures 2 & 3: the increasing prevalence of red clump stars at higher lithium enhancement points to an event between the red giant branch and red clump phases of stellar evolution, or at the He-flash itself, that causes Li-enrichment.
- e) Figures 12, 15: we find no evidence for the role of planetary engulfment from condensation temperature or refractory element trends. However, this finding does not rule out planetary engulfment as a possible scenario for Li-enrichment, since planetary engulfment signatures are short lived, and dependent on stellar age.
- f) Figure 10: we find no difference in UV and IR emission using GALEX and WISE data, respectively, between populations of Li-rich and Li-normal stars.

Our analysis provides evidence of multiple mechanisms of Li-enrichment of red giants, including both internal and external modes. Our work provides direct evidence that a subset of Li-rich stars are preferentially in binary systems, and a subset have likely undergone mass transfer from an intermediate-mass AGB companion; we report the first evidence for systematic differences in element abundances for the Li-rich population compared to the field. We have also converged on a restricted parameter space for binarity for the majority of the binary architectures, using the complementary *Gaia* measurements for the GALAH stars. We discover a most interesting result that the origin of Ba-enriched stars, which is likely low-mass AGB transfer, precludes Li-enrichment.

Lastly, we find increasing red clump membership for higher Li-enriched stars, which suggests a He-flash induced lithium production; however, the data do not differentiate between production *by* the He-flash, or from tidal-locking triggered CF production from a companion on the red clump (e.g, Casey et al. 2019). One outstanding issue with the former, as noted by Casey et al. (2019), is the origin of the required He-3 reservoir and transportation of beryllium at temperatures where lithium could be created and persist post He-flash. Conversely, an issue with the latter is that we do not detect a substantial number of binary companions for the Li-rich stars in excess of the reference Li-normal population. However, companions could be evading detection at separations just outside of and interior to the sensitivity of radial velocity and astronomy detection limits with **paired** and RUWE, respectively.

Further investigation of our sample, such as by measuring rotation periods from time-series observations, differentiating between intrinsically higher rotation and binarity, and simulating binary architectures, would enable us to model and differentiate between the roles of these different mechanisms that we are tapping into in more detail.

## 6. ACKNOWLEDGMENTS

We are thankful for helpful discussions with Jamie Tayar, Meredith Joyce, Joel Zinn, and Alex Ji. MS would like to acknowledge the support of the Natural Sciences and Engineering Research Council of Canada (NSERC). Nous remercions le Conseil de recherches en sciences naturelles et en génie du Canada (CRSNG) de son soutien. MS thanks the LSSTC Data Science Fellowship Program, which is funded by LSSTC, NSF Cybertraining Grant #1829740, the Brinson Foundation, and the Moore Foundation; her participation in the program has benefited this work. SLM acknowledges the support of the Australian Research Council through Discovery Project grant DP180101791 and the support of the UNSW Scientia Fellowship Program. This work was supported by the Australian Research Council Centre of Excellence for All Sky Astrophysics in 3 Dimensions (ASTRO 3D), through project number CE170100013. B.D.M. is supported in part by the National Science Foundation through the NSF-BSF program (grant number AST-2009255). The Flatiron Institute is supported by the Simons Foundation.

This work made use of the Third Data Release of the GALAH Survey (Buder et al. 2021). The GALAH Survey is based on data acquired through the

Australian Astronomical Observatory, under programs: A/2013B/13 (The GALAH pilot survey); A/2014A/25, A/2015A/19, A2017A/18 (The GALAH survey phase 1); A2018A/18 (Open clusters with HERMES); A2019A/1 (Hierarchical star formation in Ori OB1); A2019A/15 (The GALAH survey phase 2); A/2015B/19, A/2016A/22, A/2016B/10, A/2017B/16, A/2018B/15 (The HERMES-TESS program); and A/2015A/3, A/2015B/1, A/2015B/19, A/2016A/22, A/2016B/12, A/2017A/14 (The HERMES K2-follow-up program). We acknowledge the traditional owners of the land on which the AAT stands, the Gamilaraay people, and pay our respects to elders past and present. This paper includes data that has been provided by AAO Data Central ([datacentral.org.au](http://datacentral.org.au)).

This work has made use of data from the European Space Agency (ESA) mission *Gaia* (<https://www.cosmos.esa.int/gaia>), processed by the *Gaia* Data Processing and Analysis Consortium (DPAC, <https://www.cosmos.esa.int/web/gaia/dpac/consortium>). Funding for the DPAC has been provided by national institutions, in particular the institutions participating in the *Gaia* Multilateral Agreement. This paper makes use of data products from the Wide-field Infrared Survey Explorer, which is a joint project of the University of California, Los Angeles, and the Jet Propulsion Laboratory/California Institute of Technology, funded by the National Aeronautics and Space Administration.

*Facilities:* *Gaia* (Gaia Collaboration et al. 2016, 2018, 2022), GALAH (De Silva et al. 2015; Buder et al. 2021), GALEX (Martin et al. 2005; Bianchi et al. 2017)

*Software:* astropy (Astropy Collaboration et al. 2013, 2018), Matplotlib (Hunter 2007), NumPy (Harris et al. 2020), Pandas (Wes McKinney 2010), SciPy (Virtanen et al. 2020)

## APPENDIX

### A. YTTRIUM, ZIRCONIUM AND LANTHANAM DISTRIBUTIONS OF Li-rich AND DOPPELGÄNGERS

Figure 19 shows the distribution of three *s*-process elements where we see a group of doppelgängers with

high *s*-process abundance compared to their Li-rich counterpart, similar to the distribution seen for barium in Figure 14.

## REFERENCES

- Adamów, M., Niedzielski, A., Villaver, E., Nowak, G., & Wolszczan, A. 2012, *ApJL*, 754, L15, doi: [10.1088/2041-8205/754/1/L15](https://doi.org/10.1088/2041-8205/754/1/L15)
- Adamów, M., Niedzielski, A., Villaver, E., Wolszczan, A., & Nowak, G. 2014, *A&A*, 569, A55, doi: [10.1051/0004-6361/201423400](https://doi.org/10.1051/0004-6361/201423400)



**Table 5.** Survey identification information for 1155 Li-rich stars in our sample. GALAH IDs are `subject_id` in Buder et al. (2021), and GALEX IDs are `objid` in Bianchi et al. (2017). The full table in machine-readable format can be found online.

GALAH ID	<i>Gaia</i> DR2 ID	<i>Gaia</i> DR3 ID	GALEX ID
131118002901313	4769316162914833024	4769316162914833024	GALEX J052639.7-570922
131123003501064	5477688834192901632	5477688834192901632	–
131218002401174	5479312744147026688	5479312744147026688	–
140112002301046	5487706347195367168	5487706347195367168	–
140209002201006	5295277759201045120	5295277759201045120	–
140209002202072	5295162821578679168	5295162821578679168	–
140303000402167	5390773299010265856	5390773299010265856	–
140307003101263	6083719092007736704	6083719092007736704	–
140309003101259	5246870110524338304	5246870110524338304	–
140309003101316	5243854867384711168	5243854867384711168	–
...	...	...	...

**Table 6.** Similar to Table 5. Survey identification information for 830 unique doppelgängers in our sample. The full table in machine-readable format can be found online.

GALAH ID	<i>Gaia</i> DR2 ID	<i>Gaia</i> DR3 ID	GALEX ID
131216002101079	5292758159585894656	5292758159585894656	–
131216002101179	5293640655106197248	5293640655106197248	–
140112002301022	5487851345291190400	5487851345291190400	–
140114003701129	5486168920701339136	5486168920701339136	–
140116003202072	5488023728098978304	5488023728098978304	–
140117001501255	3323242146556260224	3323242146556260224	–
140118002501064	3119510445888798592	3119510445888798592	–
140209001701249	2967041855658375808	2967041855658375808	–
140209002201009	5295432893419869696	5295432893419869696	–
140209002201066	5295221615388716928	5295221615388716928	–

Aguilera-Gómez, C., Chanamé, J., Pinsonneault, M. H., & Carlberg, J. K. 2016a, *ApJL*, 833, L24, doi: [10.3847/2041-8213/833/2/L24](https://doi.org/10.3847/2041-8213/833/2/L24)

—. 2016b, *ApJ*, 829, 127, doi: [10.3847/0004-637X/829/2/127](https://doi.org/10.3847/0004-637X/829/2/127)

Aguilera-Gómez, C., Monaco, L., Mucciarelli, A., et al. 2022, *A&A*, 657, A33, doi: [10.1051/0004-6361/202141750](https://doi.org/10.1051/0004-6361/202141750)

Ahumada, R., Prieto, C. A., Almeida, A., et al. 2020, *ApJS*, 249, 3, doi: [10.3847/1538-4365/ab929e](https://doi.org/10.3847/1538-4365/ab929e)

Alexander, J. B. 1967, *The Observatory*, 87, 238

Asplund, M., Grevesse, N., Sauval, A. J., & Scott, P. 2009, *ARA&A*, 47, 481, doi: [10.1146/annurev.astro.46.060407.145222](https://doi.org/10.1146/annurev.astro.46.060407.145222)

Astropy Collaboration, Robitaille, T. P., Tollerud, E. J., et al. 2013, *A&A*, 558, A33, doi: [10.1051/0004-6361/201322068](https://doi.org/10.1051/0004-6361/201322068)

Astropy Collaboration, Price-Whelan, A. M., Sipőcz, B. M., et al. 2018, *AJ*, 156, 123, doi: [10.3847/1538-3881/aabc4f](https://doi.org/10.3847/1538-3881/aabc4f)

Balachandran, S. C., Fekel, F. C., Henry, G. W., & Uitenbroek, H. 2000, *ApJ*, 542, 978, doi: [10.1086/317055](https://doi.org/10.1086/317055)

Baumann, P., Ramírez, I., Meléndez, J., Asplund, M., & Lind, K. 2010, *A&A*, 519, A87, doi: [10.1051/0004-6361/201015137](https://doi.org/10.1051/0004-6361/201015137)

Bedell, M., Bean, J. L., Meléndez, J., et al. 2018, *ApJ*, 865, 68, doi: [10.3847/1538-4357/aad908](https://doi.org/10.3847/1538-4357/aad908)

Behrard, A., Dai, F., Brewer, J. M., Berger, T. A., & Howard, A. W. 2022a, arXiv e-prints, arXiv:2210.12121. <https://arxiv.org/abs/2210.12121>

Behrard, A., Sevilla, J., & Fuller, J. 2022b, arXiv e-prints, arXiv:2210.11679. <https://arxiv.org/abs/2210.11679>

Belokurov, V., Penoyre, Z., Oh, S., et al. 2020, *MNRAS*, 496, 1922, doi: [10.1093/mnras/staa1522](https://doi.org/10.1093/mnras/staa1522)

Berger, T. A., Huber, D., van Saders, J. L., et al. 2020, *AJ*, 159, 280, doi: [10.3847/1538-3881/159/6/280](https://doi.org/10.3847/1538-3881/159/6/280)

Bianchi, L., Shiao, B., & Thilker, D. 2017, *ApJS*, 230, 24, doi: [10.3847/1538-4365/aa7053](https://doi.org/10.3847/1538-4365/aa7053)

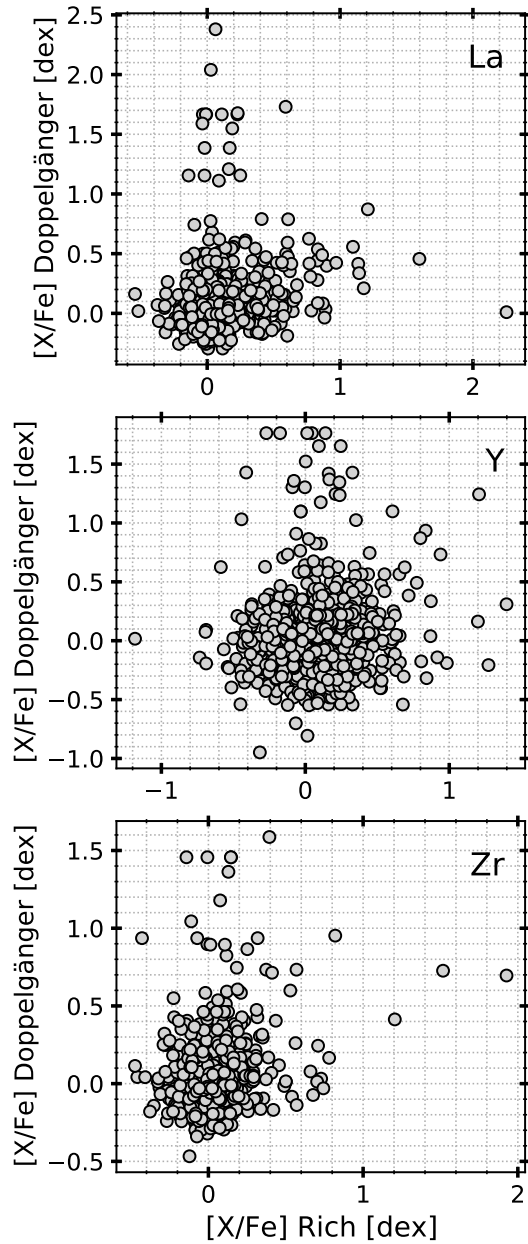


**Figure 19.** Comparing distribution of  $s$ -process elements (La, Y, and Zr) between the Li-rich (x-axis) and doppelgänger (y-axis) samples.

Boesgaard, A. M., & Krugler Hollek, J. 2009, *ApJ*, 691, 1412, doi: [10.1088/0004-637X/691/2/1412](https://doi.org/10.1088/0004-637X/691/2/1412)

Brown, J. A., Sneden, C., Lambert, D. L., & Dutchover, Edward, J. 1989, *ApJS*, 71, 293, doi: [10.1086/191375](https://doi.org/10.1086/191375)

Buder, S. 2019, PhD thesis, Ruprecht-Karls University of Heidelberg, Germany

Buder, S., Sharma, S., Kos, J., et al. 2021, *MNRAS*, 506, 150, doi: [10.1093/mnras/stab1242](https://doi.org/10.1093/mnras/stab1242)

Busso, M., Wasserburg, G. J., Nollett, K. M., & Calandra, A. 2007, *ApJ*, 671, 802, doi: [10.1086/522616](https://doi.org/10.1086/522616)

Cameron, A. G. W., & Fowler, W. A. 1971, *ApJ*, 164, 111, doi: [10.1086/150821](https://doi.org/10.1086/150821)

Cantiello, M., & Langer, N. 2010, *A&A*, 521, A9, doi: [10.1051/0004-6361/20101430510.48550/arXiv.1006.1354](https://doi.org/10.1051/0004-6361/20101430510.48550/arXiv.1006.1354)

Carlberg, J. K., Smith, V. V., Cunha, K., Majewski, S. R., & Rood, R. T. 2010, *ApJL*, 723, L103, doi: [10.1088/2041-8205/723/1/L103](https://doi.org/10.1088/2041-8205/723/1/L103)

Carney, B. W., Gray, D. F., Yong, D., et al. 2008, *AJ*, 135, 892, doi: [10.1088/0004-6256/135/3/892](https://doi.org/10.1088/0004-6256/135/3/892)

Casey, A. R., Ruchti, G., Masseron, T., et al. 2016, *MNRAS*, 461, 3336, doi: [10.1093/mnras/stw1512](https://doi.org/10.1093/mnras/stw1512)

Casey, A. R., Ho, A. Y. Q., Ness, M., et al. 2019, *ApJ*, 880, 125, doi: [10.3847/1538-4357/ab27bf](https://doi.org/10.3847/1538-4357/ab27bf)

Chambers, J. E. 2010, *ApJ*, 724, 92, doi: [10.1088/0004-637X/724/1/92](https://doi.org/10.1088/0004-637X/724/1/92)

Chanamé, J., Pinsonneault, M. H., Aguilera-Gómez, C., & Zinn, J. C. 2022, *ApJ*, 933, 58, doi: [10.3847/1538-4357/ac70c8](https://doi.org/10.3847/1538-4357/ac70c8)

Chance, Q., Foreman-Mackey, D., Ballard, S., et al. 2022, arXiv e-prints, arXiv:2206.11275. <https://arxiv.org/abs/2206.11275>

Charbonnel, C., & Balachandran, S. C. 2000, *A&A*, 359, 563. <https://arxiv.org/abs/astro-ph/0005280>

Charbonnel, C., & Lagarde, N. 2010, *A&A*, 522, A10, doi: [10.1051/0004-6361/201014432](https://doi.org/10.1051/0004-6361/201014432)

Cropper, M., Katz, D., Sartoretti, P., et al. 2018, *A&A*, 616, A5, doi: [10.1051/0004-6361/201832763](https://doi.org/10.1051/0004-6361/201832763)

Cseh, B., Lugaro, M., D’Orazi, V., et al. 2018, *A&A*, 620, A146, doi: [10.1051/0004-6361/201834079](https://doi.org/10.1051/0004-6361/201834079)

Cseh, B., Világos, B., Roriz, M. P., et al. 2022, *A&A*, 660, A128, doi: [10.1051/0004-6361/202142468](https://doi.org/10.1051/0004-6361/202142468)

Cutri, R. M., & et al. 2012, *VizieR Online Data Catalog*, II/311

da Silva, R., Milone, A. d. C., & Rocha-Pinto, H. J. 2015, *A&A*, 580, A24, doi: [10.1051/0004-6361/201525770](https://doi.org/10.1051/0004-6361/201525770)

De Silva, G. M., Freeman, K. C., Bland-Hawthorn, J., et al. 2015, *MNRAS*, 449, 2604, doi: [10.1093/mnras/stv327](https://doi.org/10.1093/mnras/stv327)

Dearborn, D. S. P., Schramm, D. N., Steigman, G., & Truran, J. 1989, *ApJ*, 347, 455, doi: [10.1086/168133](https://doi.org/10.1086/168133)

Deepak, & Lambert, D. L. 2021a, *MNRAS*, 505, 642, doi: [10.1093/mnras/stab1195](https://doi.org/10.1093/mnras/stab1195)

—. 2021b, *MNRAS*, 507, 205, doi: [10.1093/mnras/stab2022](https://doi.org/10.1093/mnras/stab2022)

Deepak, Lambert, D. L., & Reddy, B. E. 2020, *MNRAS*, 494, 1348, doi: [10.1093/mnras/staa729](https://doi.org/10.1093/mnras/staa729)

Deepak, & Reddy, B. E. 2019, *MNRAS*, 484, 2000, doi: [10.1093/mnras/stz128](https://doi.org/10.1093/mnras/stz128)

- Delgado Mena, E., Israelian, G., González Hernández, J. I., et al. 2014, *A&A*, 562, A92, doi: [10.1051/0004-6361/201321493](https://doi.org/10.1051/0004-6361/201321493)
- Delgado Mena, E., Tsantaki, M., Sousa, S. G., et al. 2016, *A&A*, 587, A66, doi: [10.1051/0004-6361/201527196](https://doi.org/10.1051/0004-6361/201527196)
- den Hartogh, J. W., Yagüe López, A., Cseh, B., et al. 2022, arXiv e-prints, arXiv:2212.03593. <https://arxiv.org/abs/2212.03593>
- Denissenkov, P. A., & Herwig, F. 2004, *ApJ*, 612, 1081, doi: [10.1086/422575](https://doi.org/10.1086/422575)
- Dixon, D., Tayar, J., & Stassun, K. G. 2020, *AJ*, 160, 12, doi: [10.3847/1538-3881/ab9080](https://doi.org/10.3847/1538-3881/ab9080)
- D’Orazi, V., Gratton, R. G., Angelou, G. C., et al. 2015a, *ApJL*, 801, L32, doi: [10.1088/2041-8205/801/2/L32](https://doi.org/10.1088/2041-8205/801/2/L32)
- . 2015b, *MNRAS*, 449, 4038, doi: [10.1093/mnras/stv612](https://doi.org/10.1093/mnras/stv612)
- Escorza, A., & De Rosa, R. J. 2023, arXiv e-prints, arXiv:2301.04232. <https://arxiv.org/abs/2301.04232>
- Evans, D. W., Riello, M., De Angeli, F., et al. 2018, *A&A*, 616, A4, doi: [10.1051/0004-6361/201832756](https://doi.org/10.1051/0004-6361/201832756)
- Findeisen, K., & Hillenbrand, L. 2010, *AJ*, 139, 1338, doi: [10.1088/0004-6256/139/4/1338](https://doi.org/10.1088/0004-6256/139/4/1338)
- Findeisen, K., Hillenbrand, L., & Soderblom, D. 2011, *AJ*, 142, 23, doi: [10.1088/0004-6256/142/1/23](https://doi.org/10.1088/0004-6256/142/1/23)
- Gaia Collaboration, Prusti, T., de Bruijne, J. H. J., et al. 2016, *A&A*, 595, A1, doi: [10.1051/0004-6361/201629272](https://doi.org/10.1051/0004-6361/201629272)
- Gaia Collaboration, Brown, A. G. A., Vallenari, A., et al. 2018, *A&A*, 616, A1, doi: [10.1051/0004-6361/201833051](https://doi.org/10.1051/0004-6361/201833051)
- Gaia Collaboration, Vallenari, A., Brown, A. G. A., et al. 2022, arXiv e-prints, arXiv:2208.00211. <https://arxiv.org/abs/2208.00211>
- Gao, Q., Shi, J.-R., Yan, H.-L., et al. 2019, *ApJS*, 245, 33, doi: [10.3847/1538-4365/ab505c](https://doi.org/10.3847/1538-4365/ab505c)
- Gao, X., Lind, K., Amarsi, A. M., et al. 2020, *MNRAS*, 497, L30, doi: [10.1093/mnras/laaa109](https://doi.org/10.1093/mnras/laaa109)
- Gilmore, G., Edvardsson, B., & Nissen, P. E. 1991, *ApJ*, 378, 17, doi: [10.1086/170402](https://doi.org/10.1086/170402)
- Giribaldi, R. E., & Smiljanic, R. 2022, *Experimental Astronomy*, doi: [10.1007/s10686-022-09850-z](https://doi.org/10.1007/s10686-022-09850-z)
- Gonzalez, G., Carlson, M. K., & Tobin, R. W. 2010, *MNRAS*, 407, 314, doi: [10.1111/j.1365-2966.2010.16900.x](https://doi.org/10.1111/j.1365-2966.2010.16900.x)
- Gonzalez, O. A., Zoccali, M., Monaco, L., et al. 2009, *A&A*, 508, 289, doi: [10.1051/0004-6361/200912469](https://doi.org/10.1051/0004-6361/200912469)
- Gray, D. F. 1980, *ApJ*, 235, 508, doi: [10.1086/157653](https://doi.org/10.1086/157653)
- Griffith, E. J., Weinberg, D. H., Buder, S., et al. 2022, *ApJ*, 931, 23, doi: [10.3847/1538-4357/ac5826](https://doi.org/10.3847/1538-4357/ac5826)
- Guandalini, R., Palmerini, S., Busso, M., & Uttenthaler, S. 2009, *PASA*, 26, 168, doi: [10.1071/AS08063](https://doi.org/10.1071/AS08063)
- Hansen, T. T., Andersen, J., Nordström, B., et al. 2016, *A&A*, 588, A3, doi: [10.1051/0004-6361/201527409](https://doi.org/10.1051/0004-6361/201527409)
- Harris, C. R., Millman, K. J., van der Walt, S. J., et al. 2020, *Nature*, 585, 357, doi: [10.1038/s41586-020-2649-2](https://doi.org/10.1038/s41586-020-2649-2)
- Heiter, U., Weiss, W. W., & Paurzen, E. 2002, *A&A*, 381, 971, doi: [10.1051/0004-6361:20011594](https://doi.org/10.1051/0004-6361:20011594)
- Hunter, J. D. 2007, *Computing in Science & Engineering*, 9, 90, doi: [10.1109/MCSE.2007.55](https://doi.org/10.1109/MCSE.2007.55)
- Iben, Icko, J. 1968, *ApJ*, 154, 581, doi: [10.1086/149782](https://doi.org/10.1086/149782)
- Israelian, G., Santos, N. C., Mayor, M., & Rebolo, R. 2004, *A&A*, 414, 601, doi: [10.1051/0004-6361:20034398](https://doi.org/10.1051/0004-6361:20034398)
- Israelian, G., Delgado Mena, E., Santos, N. C., et al. 2009, *Nature*, 462, 189, doi: [10.1038/nature08483](https://doi.org/10.1038/nature08483)
- Izzo, L., Della Valle, M., Mason, E., et al. 2015, *ApJL*, 808, L14, doi: [10.1088/2041-8205/808/1/L14](https://doi.org/10.1088/2041-8205/808/1/L14)
- Johnson, J. A., Aller, K. M., Howard, A. W., & Crepp, J. R. 2010, *PASP*, 122, 905, doi: [10.1086/655775](https://doi.org/10.1086/655775)
- Jorissen, A., & Mayor, M. 1988, *A&A*, 198, 187
- Jorissen, A., Van Eck, S., Mayor, M., & Udry, S. 1998, *A&A*, 332, 877, doi: [10.48550/arXiv.astro-ph/9801272](https://doi.org/10.48550/arXiv.astro-ph/9801272)
- Karakas, A. I., Marino, A. F., & Nataf, D. M. 2014, *ApJ*, 784, 32, doi: [10.1088/0004-637X/784/1/32](https://doi.org/10.1088/0004-637X/784/1/32)
- King, J. R., Deliyannis, C. P., Hiltgen, D. D., et al. 1997, *AJ*, 113, 1871, doi: [10.1086/118399](https://doi.org/10.1086/118399)
- Kirby, E. N., Fu, X., Guhathakurta, P., & Deng, L. 2012a, *ApJL*, 752, L16, doi: [10.1088/2041-8205/752/1/L16](https://doi.org/10.1088/2041-8205/752/1/L16)
- . 2012b, *ApJL*, 752, L16, doi: [10.1088/2041-8205/752/1/L16](https://doi.org/10.1088/2041-8205/752/1/L16)
- Kirby, E. N., Guhathakurta, P., Zhang, A. J., et al. 2016, *ApJ*, 819, 135, doi: [10.3847/0004-637X/819/2/135](https://doi.org/10.3847/0004-637X/819/2/135)
- Koch, A., Lind, K., & Rich, R. M. 2011, *ApJL*, 738, L29, doi: [10.1088/2041-8205/738/2/L29](https://doi.org/10.1088/2041-8205/738/2/L29)
- Koch, A., Lind, K., Thompson, I. B., & Rich, R. M. 2012, *Memorie della Societa Astronomica Italiana Supplementi*, 22, 79. <https://arxiv.org/abs/1203.6079>
- Kowkabany, J., Ezzeddine, R., Charbonnel, C., et al. 2022, arXiv e-prints, arXiv:2209.02184. <https://arxiv.org/abs/2209.02184>
- Kraft, R. P. 1967, *ApJ*, 150, 551, doi: [10.1086/149359](https://doi.org/10.1086/149359)
- Kumar, Y. B., Reddy, B. E., Campbell, S. W., et al. 2020, *Nature Astronomy*, 4, 1059, doi: [10.1038/s41550-020-1139-7](https://doi.org/10.1038/s41550-020-1139-7)
- Kumar, Y. B., Reddy, B. E., & Lambert, D. L. 2011, *ApJL*, 730, L12, doi: [10.1088/2041-8205/730/1/L12](https://doi.org/10.1088/2041-8205/730/1/L12)
- Lanzafame, A. C., Brugaletta, E., Frémat, Y., et al. 2022, arXiv e-prints, arXiv:2206.05766. <https://arxiv.org/abs/2206.05766>
- Lebzelter, T., Uttenthaler, S., Busso, M., Schultheis, M., & Aringer, B. 2012, *A&A*, 538, A36, doi: [10.1051/0004-6361/201117743](https://doi.org/10.1051/0004-6361/201117743)
- Li, H., Aoki, W., Matsuno, T., et al. 2018, *ApJL*, 852, L31, doi: [10.3847/2041-8213/aaa438](https://doi.org/10.3847/2041-8213/aaa438)

- Lindegren, L., Hernández, J., Bombrun, A., et al. 2018, *A&A*, 616, A2, doi: [10.1051/0004-6361/201832727](https://doi.org/10.1051/0004-6361/201832727)
- Liu, F., Asplund, M., Ramirez, I., Yong, D., & Melendez, J. 2014, *MNRAS*, 442, L51, doi: [10.1093/mnrasl/slu055](https://doi.org/10.1093/mnrasl/slu055)
- Liu, F., Yong, D., Asplund, M., et al. 2020, *MNRAS*, 495, 3961, doi: [10.1093/mnras/staa1420](https://doi.org/10.1093/mnras/staa1420)
- Lodders, K. 2003, *ApJ*, 591, 1220, doi: [10.1086/375492](https://doi.org/10.1086/375492)
- Maas, T., Van Winckel, H., & Lloyd Evans, T. 2005, *A&A*, 429, 297, doi: [10.1051/0004-6361:20041688](https://doi.org/10.1051/0004-6361:20041688)
- Magrini, L., Lagarde, N., Charbonnel, C., et al. 2021, *A&A*, 651, A84, doi: [10.1051/0004-6361/202140935](https://doi.org/10.1051/0004-6361/202140935)
- Mallik, A., Singh, R., & Reddy, B. E. 2023, arXiv e-prints, arXiv:2301.10436, doi: [10.48550/arXiv.2301.10436](https://doi.org/10.48550/arXiv.2301.10436)
- Mallik, S. V. 1997, *A&AS*, 124, 359, doi: [10.1051/aas:1997199](https://doi.org/10.1051/aas:1997199)
- Martell, S. L., & Shetrone, M. D. 2013, *MNRAS*, 430, 611, doi: [10.1093/mnras/sts661](https://doi.org/10.1093/mnras/sts661)
- Martell, S. L., Simpson, J. D., Balasubramaniam, A. G., et al. 2021, *MNRAS*, 505, 5340, doi: [10.1093/mnras/stab1356](https://doi.org/10.1093/mnras/stab1356)
- Martin, D. C., Fanson, J., Schiminovich, D., et al. 2005, *ApJL*, 619, L1, doi: [10.1086/426387](https://doi.org/10.1086/426387)
- McClure, R. D. 1983, *ApJ*, 268, 264, doi: [10.1086/160951](https://doi.org/10.1086/160951)
- . 1984, *PASP*, 96, 117, doi: [10.1086/131310](https://doi.org/10.1086/131310)
- McClure, R. D., Fletcher, J. M., & Nemeč, J. M. 1980, *ApJL*, 238, L35, doi: [10.1086/183252](https://doi.org/10.1086/183252)
- McClure, R. D., & Woodsworth, A. W. 1990, *ApJ*, 352, 709, doi: [10.1086/168573](https://doi.org/10.1086/168573)
- Meléndez, J., Asplund, M., Gustafsson, B., & Yong, D. 2009, *ApJL*, 704, L66, doi: [10.1088/0004-637X/704/1/L66](https://doi.org/10.1088/0004-637X/704/1/L66)
- Meléndez, J., Bergemann, M., Cohen, J. G., et al. 2012, *A&A*, 543, A29, doi: [10.1051/0004-6361/201117222](https://doi.org/10.1051/0004-6361/201117222)
- Meléndez, J., Bedell, M., Bean, J. L., et al. 2017, *A&A*, 597, A34, doi: [10.1051/0004-6361/201527775](https://doi.org/10.1051/0004-6361/201527775)
- Metzger, B. D., Giannios, D., & Spiegel, D. S. 2012, *MNRAS*, 425, 2778, doi: [10.1111/j.1365-2966.2012.21444.x](https://doi.org/10.1111/j.1365-2966.2012.21444.x)
- Ming-hao, D., Shao-lan, B., Jian-rong, S., & Hong-liang, Y. 2021, *ChA&A*, 45, 45, doi: [10.1016/j.chinastron.2021.02.003](https://doi.org/10.1016/j.chinastron.2021.02.003)
- Molaro, P., Izzo, L., Mason, E., Bonifacio, P., & Della Valle, M. 2016, *MNRAS*, 463, L117, doi: [10.1093/mnrasl/slw169](https://doi.org/10.1093/mnrasl/slw169)
- Monaco, L., Villanova, S., Moni Bidin, C., et al. 2011, *A&A*, 529, A90, doi: [10.1051/0004-6361/201016285](https://doi.org/10.1051/0004-6361/201016285)
- Montes, D., Fernandez-Figueroa, M. J., Cornide, M., & de Castro, E. 1996, *A&A*, 312, 221, doi: [10.48550/arXiv.astro-ph/9511125](https://doi.org/10.48550/arXiv.astro-ph/9511125)
- Mori, K., Kusakabe, M., Balantekin, A. B., Kajino, T., & Famiano, M. A. 2021, *MNRAS*, 503, 2746, doi: [10.1093/mnras/stab595](https://doi.org/10.1093/mnras/stab595)
- Nibauer, J., Baxter, E. J., Jain, B., et al. 2021, *ApJ*, 907, 116, doi: [10.3847/1538-4357/abd0f1](https://doi.org/10.3847/1538-4357/abd0f1)
- Nieminen, T. A. 2017, arXiv e-prints, arXiv:1708.06408, doi: [10.48550/arXiv.1708.06408](https://doi.org/10.48550/arXiv.1708.06408)
- Nissen, P. E. 2015, *A&A*, 579, A52, doi: [10.1051/0004-6361/201526269](https://doi.org/10.1051/0004-6361/201526269)
- Nissen, P. E., Christensen-Dalsgaard, J., Mosumgaard, J. R., et al. 2020, *A&A*, 640, A81, doi: [10.1051/0004-6361/202038300](https://doi.org/10.1051/0004-6361/202038300)
- Nordhaus, J., Busso, M., Wasserburg, G. J., Blackman, E. G., & Palmerini, S. 2008, *ApJL*, 684, L29, doi: [10.1086/591963](https://doi.org/10.1086/591963)
- Norfolk, B. J., Casey, A. R., Karakas, A. I., et al. 2019, *MNRAS*, 490, 2219, doi: [10.1093/mnras/stz2630](https://doi.org/10.1093/mnras/stz2630)
- Noyes, R. W., Hartmann, L. W., Baliunas, S. L., Duncan, D. K., & Vaughan, A. H. 1984, *ApJ*, 279, 763, doi: [10.1086/161945](https://doi.org/10.1086/161945)
- Olive, K. A., & Schramm, D. N. 1992, *Nature*, 360, 439, doi: [10.1038/360439a0](https://doi.org/10.1038/360439a0)
- Patton, R. A., Pinsonneault, M. H., Cao, L., et al. 2023, arXiv e-prints, arXiv:2303.08151, <https://arxiv.org/abs/2303.08151>
- Petrenz, P., & Puls, J. 1996, *A&A*, 312, 195
- Ramírez, I., Meléndez, J., & Asplund, M. 2009, *A&A*, 508, L17, doi: [10.1051/0004-6361/200913038](https://doi.org/10.1051/0004-6361/200913038)
- Ramírez, I., Meléndez, J., Cornejo, D., Roederer, I. U., & Fish, J. R. 2011, *ApJ*, 740, 76, doi: [10.1088/0004-637X/740/2/76](https://doi.org/10.1088/0004-637X/740/2/76)
- Rebull, L. M., Carlberg, J. K., Gibbs, J. C., et al. 2015, *AJ*, 150, 123, doi: [10.1088/0004-6256/150/4/123](https://doi.org/10.1088/0004-6256/150/4/123)
- Reddy, B. E., & Lambert, D. L. 2005, *AJ*, 129, 2831, doi: [10.1086/430190](https://doi.org/10.1086/430190)
- Reeves, H., Fowler, W. A., & Hoyle, F. 1970, *Nature*, 226, 727, doi: [10.1038/226727a0](https://doi.org/10.1038/226727a0)
- Ruchti, G. R., Fulbright, J. P., Wyse, R. F. G., et al. 2011a, *ApJ*, 743, 107, doi: [10.1088/0004-637X/743/2/107](https://doi.org/10.1088/0004-637X/743/2/107)
- . 2011b, *ApJ*, 743, 107, doi: [10.1088/0004-637X/743/2/107](https://doi.org/10.1088/0004-637X/743/2/107)
- Rukeya, R., Lü, G., Wang, Z., & Zhu, C. 2017, *PASP*, 129, 074201, doi: [10.1088/1538-3873/aa6b4d](https://doi.org/10.1088/1538-3873/aa6b4d)
- Sackmann, I. J., & Boothroyd, A. I. 1992, *ApJL*, 392, L71, doi: [10.1086/186428](https://doi.org/10.1086/186428)
- Sahai, R., Findeisen, K., Gil de Paz, A., & Sánchez Contreras, C. 2008, *ApJ*, 689, 1274, doi: [10.1086/592559](https://doi.org/10.1086/592559)
- Sanna, N., Franciosini, E., Pancino, E., et al. 2020, *A&A*, 639, L2, doi: [10.1051/0004-6361/202038435](https://doi.org/10.1051/0004-6361/202038435)

- Savage, B. D., & Sembach, K. R. 1996, *ARA&A*, 34, 279, doi: [10.1146/annurev.astro.34.1.279](https://doi.org/10.1146/annurev.astro.34.1.279)
- Schiappacasse-Ulloa, J., Lucatello, S., Rain, M. J., & Pietrinferni, A. 2022, *MNRAS*, 511, 231, doi: [10.1093/mnras/stab3795](https://doi.org/10.1093/mnras/stab3795)
- Schuler, S. C., Flateau, D., Cunha, K., et al. 2011, *ApJ*, 732, 55, doi: [10.1088/0004-637X/732/1/55](https://doi.org/10.1088/0004-637X/732/1/55)
- Schuler, S. C., Vaz, Z. A., Katime Santrich, O. J., et al. 2015, *ApJ*, 815, 5, doi: [10.1088/0004-637X/815/1/5](https://doi.org/10.1088/0004-637X/815/1/5)
- Schwab, J. 2020, *ApJL*, 901, L18, doi: [10.3847/2041-8213/abb45f](https://doi.org/10.3847/2041-8213/abb45f)
- Sharma, S., Stello, D., Buder, S., et al. 2018, *MNRAS*, 473, 2004, doi: [10.1093/mnras/stx2582](https://doi.org/10.1093/mnras/stx2582)
- Sheinis, A., Anguiano, B., Asplund, M., et al. 2015, *Journal of Astronomical Telescopes, Instruments, and Systems*, 1, 035002, doi: [10.1117/1.JATIS.1.3.035002](https://doi.org/10.1117/1.JATIS.1.3.035002)
- Shkolnik, E. L., Liu, M. C., Reid, I. N., Dupuy, T., & Weinberger, A. J. 2011, *ApJ*, 727, 6, doi: [10.1088/0004-637X/727/1/6](https://doi.org/10.1088/0004-637X/727/1/6)
- Siess, L., & Livio, M. 1999a, *MNRAS*, 304, 925, doi: [10.1046/j.1365-8711.1999.02376.x](https://doi.org/10.1046/j.1365-8711.1999.02376.x)
- . 1999b, *MNRAS*, 308, 1133, doi: [10.1046/j.1365-8711.1999.02784.x](https://doi.org/10.1046/j.1365-8711.1999.02784.x)
- Singh, R., Reddy, B. E., Bharat Kumar, Y., & Antia, H. M. 2019, *ApJL*, 878, L21, doi: [10.3847/2041-8213/ab2599](https://doi.org/10.3847/2041-8213/ab2599)
- Smiljanic, R., da Silva, A. R., & Giribaldi, R. E. 2022, *Experimental Astronomy*, doi: [10.1007/s10686-022-09845-w](https://doi.org/10.1007/s10686-022-09845-w)
- Smith, V. V., & Lambert, D. L. 1989, *ApJL*, 345, L75, doi: [10.1086/185556](https://doi.org/10.1086/185556)
- Sneden, C., Afşar, M., Bozkurt, Z., et al. 2022, *ApJ*, 940, 12, doi: [10.3847/1538-4357/ac922e](https://doi.org/10.3847/1538-4357/ac922e)
- Soares-Furtado, M., Cantiello, M., MacLeod, M., & Ness, M. K. 2021, *AJ*, 162, 273, doi: [10.3847/1538-3881/ac273c](https://doi.org/10.3847/1538-3881/ac273c)
- Soderblom, D. R., Stauffer, J. R., Hudon, J. D., & Jones, B. F. 1993, *ApJS*, 85, 315, doi: [10.1086/191767](https://doi.org/10.1086/191767)
- Spina, L., Sharma, P., Meléndez, J., et al. 2021, *Nature Astronomy*, 5, 1163, doi: [10.1038/s41550-021-01451-8](https://doi.org/10.1038/s41550-021-01451-8)
- Stancliffe, R. J. 2021, *MNRAS*, 505, 5554, doi: [10.1093/mnras/stab1734](https://doi.org/10.1093/mnras/stab1734)
- Starrfield, S., Truran, J. W., Sparks, W. M., & Arnould, M. 1978, *ApJ*, 222, 600, doi: [10.1086/156175](https://doi.org/10.1086/156175)
- Stelzer, B., Damasso, M., Scholz, A., & Matt, S. P. 2016, *MNRAS*, 463, 1844, doi: [10.1093/mnras/stw1936](https://doi.org/10.1093/mnras/stw1936)
- Tajitsu, A., Sadakane, K., Naito, H., Arai, A., & Aoki, W. 2015, *Nature*, 518, 381, doi: [10.1038/nature14161](https://doi.org/10.1038/nature14161)
- Teske, J. K., Khanal, S., & Ramírez, I. 2016, *ApJ*, 819, 19, doi: [10.3847/0004-637X/819/1/19](https://doi.org/10.3847/0004-637X/819/1/19)
- Torra, F., Castañeda, J., Fabricius, C., et al. 2021, *A&A*, 649, A10, doi: [10.1051/0004-6361/202039637](https://doi.org/10.1051/0004-6361/202039637)
- Trimble, V. 1975, *Reviews of Modern Physics*, 47, 877, doi: [10.1103/RevModPhys.47.877](https://doi.org/10.1103/RevModPhys.47.877)
- . 1991, *A&A Rv*, 3, 1, doi: [10.1007/BF00873456](https://doi.org/10.1007/BF00873456)
- Tucci Maia, M., Meléndez, J., & Ramírez, I. 2014, *ApJL*, 790, L25, doi: [10.1088/2041-8205/790/2/L25](https://doi.org/10.1088/2041-8205/790/2/L25)
- Uttenthaler, S., Lebzelter, T., Palmerini, S., et al. 2007, *A&A*, 471, L41, doi: [10.1051/0004-6361:20077879](https://doi.org/10.1051/0004-6361:20077879)
- Venn, K. A., & Lambert, D. L. 1990, *ApJ*, 363, 234, doi: [10.1086/169334](https://doi.org/10.1086/169334)
- Ventura, P., Dell’Agli, F., Lugaro, M., et al. 2020, *A&A*, 641, A103, doi: [10.1051/0004-6361/202038289](https://doi.org/10.1051/0004-6361/202038289)
- Vigroux, L., & Arnould, M. 1979, in *Liege International Astrophysical Colloquia*, Vol. 22, *Liege International Astrophysical Colloquia*, ed. A. Boury, N. Grevesse, & L. Remy-Battiau, 47–52
- Villaver, E., & Livio, M. 2009, *ApJL*, 705, L81, doi: [10.1088/0004-637X/705/1/L81](https://doi.org/10.1088/0004-637X/705/1/L81)
- Virtanen, P., Gommers, R., Oliphant, T. E., et al. 2020, *Nature Methods*, 17, 261, doi: [10.1038/s41592-019-0686-2](https://doi.org/10.1038/s41592-019-0686-2)
- Wallerstein, G., & Conti, P. S. 1969, *ARA&A*, 7, 99, doi: [10.1146/annurev.aa.07.090169.000531](https://doi.org/10.1146/annurev.aa.07.090169.000531)
- Wallerstein, G., & Sneden, C. 1982, *ApJ*, 255, 577, doi: [10.1086/159859](https://doi.org/10.1086/159859)
- Warner, B. 1965, *MNRAS*, 129, 263, doi: [10.1093/mnras/129.3.263](https://doi.org/10.1093/mnras/129.3.263)
- Wes McKinney. 2010, in *Proceedings of the 9th Python in Science Conference*, ed. Stéfan van der Walt & Jarrod Millman, 56 – 61, doi: [10.25080/Majora-92bf1922-00a](https://doi.org/10.25080/Majora-92bf1922-00a)
- Wheeler, A. J., Hogg, D. W., & Ness, M. 2021, *ApJ*, 908, 247, doi: [10.3847/1538-4357/abd544](https://doi.org/10.3847/1538-4357/abd544)
- Wilson, O. C. 1966, *ApJ*, 144, 695, doi: [10.1086/148649](https://doi.org/10.1086/148649)
- Yan, H.-L., Shi, J.-R., Zhou, Y.-T., et al. 2018, *Nature Astronomy*, 2, 790, doi: [10.1038/s41550-018-0544-7](https://doi.org/10.1038/s41550-018-0544-7)
- Yan, H.-L., Zhou, Y.-T., Zhang, X., et al. 2021, *Nature Astronomy*, 5, 86, doi: [10.1038/s41550-020-01217-8](https://doi.org/10.1038/s41550-020-01217-8)
- Yan, T. S., Shi, J. R., Wang, L., et al. 2022, *ApJL*, 929, L14, doi: [10.3847/2041-8213/ac63a5](https://doi.org/10.3847/2041-8213/ac63a5)
- Zhou, Y., Wang, C., Yan, H., et al. 2022, *arXiv e-prints*, arXiv:2204.12759. <https://arxiv.org/abs/2204.12759>
- Zhou, Y., Yan, H., Shi, J., et al. 2019, *ApJ*, 877, 104, doi: [10.3847/1538-4357/ab1b4b](https://doi.org/10.3847/1538-4357/ab1b4b)